Enhanced sieving of cellulosic microfibers membranes via tuning of interlayer spacing

SCHOLARONE™
Manuscripts

Environmental Science Nano

ROYAL SOCIETY OF CHEMISTRY

Guidelines for Reviewers

Thank you very much for agreeing to review this manuscript for *Environmental Science: Nano*

Environmental Science: Nano is a comprehensive, high-impact source of peer-reviewed information on the design and demonstration of engineered nanomaterials for environment-based applications and on the interactions of engineered, natural, and incidental nanomaterials with biological and environmental systems. More details can be found at **rsc.li/esnano**

Environmental Science: Nano's Impact Factor is **7.704** (2018 Journal Citation Reports®)

The following manuscript has been submitted for consideration as a

FULL PAPER

Full papers must represent a significant development in the particular field, and should be judged according to originality, quality of scientific content and contribution to existing knowledge. Full papers have no page limit, but should be appropriate in length for their scientific content. Further information on article types can be found **here**. It is essential that all articles submitted to *Environmental Science: Nano* meet the significant novelty criteria; lack of novelty is sufficient reason for rejection**.** Please consider these high standards when making your recommendation to accept, revise, or reject.

We ask reviewers to examine manuscripts very carefully, and recommend rejection of articles which do not meet our novelty, quality, impact and rigor expectations. When making your recommendation please consider:

- That **the rejection rate for *Environmental Science: Nano* is currently ~85%** of submitted manuscripts.
- That **routine or incremental** work, however competently researched and reported, should not be recommended for publication.
- That it is the responsibility of authors to provide full characterisation of all nanomaterials they claim as new. Insufficiently characterised materials is a reason for rejection or resubmission. More details can be found within the **Journal Specific Guidelines** on our website.

When preparing your report, please:

- Use the **journal scope** to assess the manuscript's suitability for publication in *Environmental Science: Nano.*
- Comment on the originality, importance, impact and reliability of the science. English language and grammatical errors do not need to be discussed, except where it impedes scientific understanding.
- State clearly whether you think the paper should be accepted or rejected, giving detailed comments that will both help the Editor to make a decision on the paper and the authors to improve it.
- Inform the Editor if there is a conflict of interest, a significant part of the work you cannot review with confidence, or if parts of the work have previously been published.
- Provide your report rapidly and within the specified deadline, or inform the Editor immediately if you cannot do so. You can submit your report at **https://mc.manuscriptcentral.com/esn**

Thank you for evaluating this manuscript. Your advice as a reviewer for *Environmental Science: Nano* is greatly appreciated.

Best regards,

Professor Peter Vikesland   **Dr Sam Keltie**
Editor-in-Chief   Executive Editor
Virginia Tech, USA   Royal Society of Chemistry

Contact us

Please visit our reviewer hub for further details of our processes, policies and reviewer responsibilities as well as guidance on how to review, or click the links below.

What to do when you review

Reviewer responsibilities

Process & policies

Enhanced sieving of cellulosic microfibers membranes via tuning of interlayer spacing

Zoheb Karim[1,2],* Susanna Monti[3]*, Giovanni Barcaro[4], Anna Svedberg[1], Mohd Ayub Ansari[5], Sadaf Afrin[6]

[1]MoRe Research Örnsköldsvik AB, Box 70, SE-89122, Örnsköldsvik, Sweden

[2]Institute of Architecture and Civil Engineering, South Ural State University, Chelyabinsk, 454080, Russia

[3]CNR-ICCOM– Institute of Chemistry of Organometallic Compounds, via Moruzzi 1, 56124 Pisa, Italy

[4]CNR-IPCF–Institute for Chemical and Physical Processes, via Moruzzi 1, 56124 Pisa, Italy

[5]Department of Chemistry, Bipin Bihari College, 284001, Jhansi, India

[6]Department of Chemistry, Faculty of Chemical Sciences, Aligarh Muslim University, Aligarh 202002, India

Corresponding authors: Z.K (zoheb.karim@gmail.com)

S.M (sapeptides@gmail.com)

Abstract

Functionally active membranes made of cellulosic microfibers (CMF) have emerged as promising sorbents for the removal of nano-sized pollutants from water. The adsorption efficiency of these membranes has been increased through surface functionalization of pristine-CMF using various chemistries. Still, until now, the produced materials consist of highly dense 2D networks that make the membranes inadequate as filters because of the too short interlayer spacing. Here, we report on novel tuned CMF functionalization procedures, namely carboxylation, phosphorylation, and methylation, that can overcome this problem by modulating the interlayer separation in the 2D membranes. To test our approach, fabricated nanolaminate membranes with grafted functional groups were subjected for the separation of metal ions, dye and two drugs and separation efficiencies are being correlated with the degree of functionalization and tuned intercapillary scaping.

Keywords: Cellulosic microfibers, Interlayer scaping, Functionalization, 2D composite membarnes

1
2
3
4
5
6
7
8
9
10
11
12
13
14
15
16
17
18
19
20
21
22
23
24
25
26
27
28
29
30
31
32
33
34
35
36
37
38
39
40
41
42
43
44
45
46
47
48
49
50
51
52
53
54
55
56
57
58
59
60

Introduction

Filtration membranes are complex molecular systems that can act as selective permeable barriers to separate various types of contaminants from water depending on their size, charge, chemical affinity, and other parameters. These membranes are mainly made of supramolecular aggregates of biocompatible components whose structure and chemical composition can be modified and modulated appropriately to obtain tuned devices with improved efficiency and specificity[1,2]. Biocompatibility and eco-sustainability are two of the essential key features that these tools should possess, which suggest moving the attention towards natural compounds. The use of cellulose as the main component perfectly satisfies these requirements. Indeed, cellulose-based nanofilters have demonstrated great potential and promising performance[3,4]. This was shown by many authors too[5,6,7,8,9] including Mathew and co-workers, who demonstrated, through various experimental techniques and modeling studies, that wood-derived cellulose, both in the form of nanofibers or nanocrystals, modified with the appropriate functional groups, can be used as a functional 2D material for the separation of pollutants[10].

It was found, indeed, that the capturing process of the targeted impurities was mainly due to the concerted action of the different functional groups such as carboxyl, phosphate, hydroxyl, aldehyde, etc[11,12,13,14,15] and that by refining the functionalization of the nanocellulose matrices[16,17] (covalently, non-covalently, grafting etc.) at the sub-nano or nano scales, more efficient and specialized filters could be produced.

Moving to the general characteristics of the selected materials, comprehensive examinations of the behavior of the cellulose nanofibers/nanocrystals[18], revealed that another key feature for producing successful cellulose-based scavengers is to refine and modulate their water permeability. Dried materials assembled into highly tight 2D frameworks are ineffectual for sieving applications because they are almost impermeable to water. Nevertheless, water permeability through such tight 2D arrangements could be increased by incubation with chemicals, as done in an earlier investigation by Karim and co-workers[3]. There, a pristine cellulose nanofiber membrane was treated with acetone for 24 h, and an increase in the water flux from 0 to 25 Lm^2h^{-1} at a differential pressure of approximately 0.45 MPa was obtained. The drawback, however, was that the reactive chemicals perturbed both the structural configuration and the surface chemistry of the membranes unpredictably. A further

fundamental aspect that should be taken into account is the stability of the material in the environment selected for its applications. For example, swelling in aqueous solution imposes a limit to the material porosity that determines a dramatic restriction of the sieving performance. High porosity can lead to the irreversible degradation of membrane integrity. All these data suggest that a meticulous control of the single components is necessary to design high-specificity membranes.

In the present investigation, we have used concerted experimental-theoretical methodologies to elucidate the crucial role played by the surface functionalization of cellulosic microfibers (CMF) for controlling interfiber spacing (*d*-spacing of lattice) of membranes appropriately designed for a selective sieving performance. Polar (–OH, –COOH and –PO_4^3) and nonpolar (–CH_3) functional groups were introduced on CMF through chemical and enzymatic catalysis, and the strength of the chemicals and enzymes (i.e. hexokinase) was explored in relation to the functionalization of the CMF matrices. Furthermore, functionalized nano laminated membranes were tested for separation of metal ions, dye and drugs and their separation effecineies are being correlated with functionalization of CMF and resulted interlayer scaping.

Methods

Functionalization of microfiberollate cellulose.

CMF was purchased and then functionalized using chemicals and enzyme hexokinase. For TEMPO oxidation, CMF suspension was oxidized as discussed by Serra et al.[19]. Phosphorylation of CMF using enzyme hexokinase was performed as discussed by Bozic et al.[20]. For methylation, CMF (1 wt%) was mixed in 60 mL NaOH solution (50% m/v) for 1 h at room temperature to merselized. Detailed methods of functionalization are explained in the supplementary file. Used CMF has been previously characterized in detail[4].

Preparation of nanolaminate membranes.

Nanolaminate membranes were fabricated using vacuum-filtration, having 12.5 cm diameter of Buchner funnel. The thickness of nanolaminate membranes was controlled by changing the filtered volume of CMF. Diameter of all produced nanolaminate membranes was 12.5 cm; a detailed method for the fabrication of

1
2
3
4
5
6
7
8
9
10
11
12
13
14
15
16
17
18
19
20
21
22
23
24
25
26
27
28
29
30
31
32
33
34
35
36
37
38
39
40
41
42
43
44
45
46
47
48
49
50
51
52
53
54
55
56
57
58
59
60

functionalized membranes has been mentioned in the supplementary file (**Figure S1**) and also reported in our previous published article[4].

Characterizations of nanolaminate membranes.

A detailed characterization of all produced membranes is mentioned in the supplementary file. SEM analysis was performed using MAGELLAN 400, SEM, FEI at an acceleration voltage of 3 kV. Mutek SZP 06, MUTEK was used for the measurement of surface ζ-potential of pristine and functionalized CMF. Varian 670-IR FTIR was used for the measurement of the introduced functional groups. ^{13}C CP/MAS NMR spectra were recorded at 295±1 K in a Bruker Avance III AQS 400 SB instrument operating at 9.4 T. The ^{31}P MAS NMR spectra were recorded in a Bruker Avance instrument using a MAS rate of 10 kHz and a 4 mm probe as reported by Ghanadpour et al.[21]. X-ray diffraction measurement was performed on a D/max III X-ray diffractometer (Rigaku Tokyo, Japan), equipped with nickel-filtered Cu Kα radiation (λ = 0.15418). X-Ray photoelectron spectroscopy analysis was carried out on the PHI-TFAXPS spectrometer produced by Physical Electronics Inc. Water permeance of all produced membranes was calculated in Convergence Clean Water Flux (CWF) pilot system (**Figure S13**). BET analysis was performed using a Micromeritics ASAP 2000 instrument, and the samples were degassed at 100°C for 24 h in dry N_2 flow prior to measurements. Tensile tester (Lorentzen &Wettre, ABB, Sweden) was used for the analysis of the mechanical performance of produced nano laminated membranes. All other techniques used for the characterization of nanolaminate membranes are discussed in the supplementary file in detail.

Nanolaminate membranes performance.

All functionalized nano laminated membranes were applied for the removal of metal ions (Mg^{2+}, Cd^{2+}, Co^{2+}, Mg^{2+} and Cr^{3+}), dye (methyl blue) and drugs (porphyrin and caffeine) and detailed characterization of these impurities is mentioned in supplementary **Table S7**. Dynamic mode as well as static mode[4] of operation using Dead-End-Cell and incubation of nanolaminate membranes in model water were performed and percentage removal and adsorption capacity of functionalized membranes were calculated according to equation (i) and (ii), respectively.

4

Molecular Dynamics Simulations.

A series of molecular dynamics simulations based on a reactive force field (ReaxFF) are used to provide a detailed view, at the atomic level, of possible configurations of the three different models of functionalized cellulose (carboxylic-CMF, methyl-CMF, phosphate-CMF). These data are essential to complement, explain, and support the experimental observations. The computational models are based on a representative cellulose chain assembly developed and tested in earlier studies[22]. The present simulations are carried out to disclose the hydrophilic character of the modified CMF, its structure, dynamics, and packing capability in wet and dry conditions. The simulations analysis is focused on structural changes, ions adsorption, and solvation effects, for detail stimulation follow supplementary file.

Results and Discussion

Characterization of the functionalized membranes.

We fabricated nanolaminate membranes by modifying the CMF matrices with functional groups having different hydrophilic character, using chemical and enzymatic catalysis (**Supplementary Figure S1**). The selected moieties comprised carboxylic (–COOH), methyl (-CH$_3$), and phosphate groups (PO$_4^3$), which were introduced through enzymatic catalysis (hexokinase mediated functionalization). From now on, CMF with hydroxyls (-OH) on the surface (**Supplementary Figure S1A**) will be referred to as pristine-CMF, whereas the functionalized nanolaminate models as carboxylic-CMF, methyl-CMF, phosphate-CMF membranes (**Supplementary Figure S1**). All of the membranes prepared using vacuum-filtration self-assembled as horizontally stacked microfibers[3,23]. A Scanning Electron Microscopy (SEM) image of the CMF after freeze-drying is shown in **Figure 1(A) and Figure S2**, whereas a picture of a typically fabricated membrane is displayed in **Figure 1(B)**. The high stability of CMF in solution translates into a highly uniform membrane with no pinholes under the surface (**Figure 1C**). Indeed, the examination of the cross-section obtained by SEM suggests that CMF self-assembled in horizontal direction (**Figure 1D)**.

The surface ζ-potential of the modified CMFs, shown in **Figure S3,** indicates highly negative surface properties of phosphate-CMF followed by carboxylic-CMF and pristine-CMF. Instead, Methyl-CMF, which has nonpolar functional groups (CH$_3$),

exhibits a positive surface ζ-potential up to pH 6.0 (**Figure S3**). The functional groups density, reported in **Supplementary Table S1,** denotes a progressive decrease as a function of the polarity of the substituents (i.e. phosphate-CMF > carboxylic-CMF > pristine-CMF). In parallel, $12.21 \pm 3.1 \mu mole/g$ of methyl density was calculated for the methylation of CMF (**Supplementary Table S1**).

A complete characterization of the membranes was accomplished through IR spectroscopy, potentiometric titration, and ^{13}C cross-polarization magic angle spinning magnetic resonance (CP MAS NMR). The stability of the functionalization (attachment of functional groups on CMF) was checked through infrared spectroscopy (**Supplementary Figure S4**) and the amount of the available functional groups by potentiometric titration (**Supplementary Table S1)**. CP MAS NMR was used to compare the chemical shift on the C6 carbon of the various cellulose samples (**Supplementary Figure S6)**. For the pristine-CMF membranes, the typical signals of cellulose appear at 107 ppm (C1), 76 and 73 (C2, C3, and C5) and 66.6 and 64.4 ppm (C6). A new peak at 176 ppm is ascribed to the sodium carboxylate carbons in the oxidized cellulose when compared to the pristine-CMF. Carboxylic-CMF membranes had nearly no influence on the chemical shift and the pattern of C1 or C4. However, the oxidized CMF has significant resonance peaks due to the original C6 primary alcohol groups of the glucose at about 67.3 ppm. On the contrary, the signal at 64.4 ppm for the C6 carbon observed for the pristine-CMFdecreases and disappears, which indicates selective oxidation of the primary OH-units (**Supplementary Figure S6**). By comparing the spectra of hexokinase-ATP treatment, it was found that the chemical shift of C6 moved from 65.5 to 55.2 ppm after its substitution with a phosphate group (**Supplementary Figure S7**). The methylated membranes have four resonance lines divided into three different spectral ranges (105, 85/75 and 60 ppm), which can be distinguished in the ^{13}C NMR spectrum.

Figure 1

The structure of functionalized nanolaminate membranes was also analyzed using X-ray Diffraction (XRD) and contact angle measurements. In the case of pristine-CMF, an intense XRD peak can be easily detected at 22.2° and attributed to the interlaminate spacing (crystal structure of pristine-CMF). The (002) peak is slightly shifted for the functionalized membranes compared to the pristine-CMF one, and the

highest shift was recorded for the phosphate-CMF case (+5.76 Å). The details of the interlayer spacing of all functionalized samples are reported in **Table S3**. The shifts of peaks at 002 indicate a broadening of the interfiber spacing due to the grafted functional groups (**Figure 2A**). It is worth mentioning that the peak at 22.2° completely disappears after the modification of the microcrystalline fibers, suggesting their complete functionalization. A theoretical estimate of the interlaminate spacing of pristine-CMF suggests average values around 4.4 Å and after functionalization an increase of about 3 Å at most, which is confirmed by the XRD image of **Figure 2A.** Consequently, the putative extensions of the grafted functional groups are in the following order: phosphate > methyl > carboxylic > hydroxyl. From the analysis of the simulations it was found that the differences between phosphate and methyl group lengths were subtle and could not be accurately estimated especially when they were packed in the dry fiber networks. Phosphate side chains seemed more pliable and could more easily rearrange according to the surrounding species, whereas methyl groups showed the tendency to adopt more rigid orientations. Inspection of the effect of surrounding moieties on the flexibility of phosphate- and methyl-CMF (**Figure S12**) in wet conditions was also examined, and it was found that a greater number of solvent molecules surrounded the phosphate-CMF compared to methylated sample (**Figure S12**) makes phosphate-CMF more flexible resulted in broader interlayer spacing compared to methyl-CMF.

As far as the water droplet contact angle is concerned, it was found that the pristine-CMF nano-laminated membrane had a 29° contact angle, which is quite low if compared with the methylated sample (76°). This was the highest value and is in line with the hydrophobic character of the methyl substituents (**Figure 2B**). In fact, the decrease in the contact angle follows the hydrophilicity of the introduced moieties (PO_4^{3}) > COOH) > OH > CH_3. Furthermore, the density of the functional groups (**Table S1**) has a direct impact on the contact angle analysis determining at high values a decrease in the contact angles.

As already mentioned above, one of the main limitations to the use of CMF based membranes is their tendency to swell in water, which deteriorates the sieving performance and renders them not appropriate for separating small molecules like dyes or metal ions. For this reason, affinity membranes are usually preferred[4].

The designed membranes formed by functionalized CMF nanolaminates showed, instead, an increase of interlaminate spacing, hence, a limited swelling during

immersion in water (**Figure 2D**). The swelling behavior of pristine and functionalized CMF membranes as a function of time is shown in **Figure 2D**. There, it is evident that the pristine-CMF membrane has the highest swelling, whereas the methyl-CMF membranes the lowest. It is worth mentioning that high hydrophilicity and flexibility of phosphorylated CMF make these membranes less propense to swell compared to their native counterpart (**Figure 2D**).

Figure 2

Ions transport and water flux

A straightforward and highly effective experimental setup, shown in **Figure S13,** was used for examining the transportation of selected ions through the functionalized nanolaminate membranes, choosing LiCl, NaCl, and KCl ionic solutions as model systems. According to the literature, the hydrated ion diameters of K^+, Na^+, and Li^+ are 6.6 Å, 7.1 Å, and 7.6 Å, respectively[24]. The intercapillary space of pristine- and carboxylic-CMF membranes was approximately 4.4 and 5.3 Å, respectively (slight increase in interlaminar space was recorded after TEMPO functionalization of the pristine-CMF), and, thus, transportation of the ions was blocked by the narrow capillary distribution. On the contrary, an increased permeation rate was recorded for the phosphorylated and methyl-CMF models with a simultaneous increase in the ionic strength. The broadest intercapillary space was recorded for the phosphate-CMF system (11.4Å) (broader opening for ions transportation through membranes) (**Figure S12**), which showed the highest transportation rate. This was followed by methyl-CMF membranes (**Figure 3**). Although the dominant effect for the high transportation rate was due to the intercapillary separation, even though other factors such as the electrostatic interactions and the binding energy could influence the ionic motion[2]. From the examination of the methyl-CMF membrane, it was noticed that this had a higher ionic permeation rate compared to the phosphate-CMF system for all the targeted ions (**Figure 3B**) having a shorter capillary width (6.8 against 11.4 Å of the phosphate-CMF). We could speculate, by considering the charge character of these two types of membranes and the results of previous simulations that the high ionic permeation of the methyl-CMF system might be ascribed to the weaker interactions between the ions and the methyl groups of the filters.

In terms of thickness, it was found, as expected, an increase from 50 to 150 µm

(**Figure 3C**), which determined a decrease in water permeability[26,27]. A very low water permeability (9 $Lh^{-1}m^{-2}bar^{-1}$) was observed for the pristine-CMF membranes and the highest for the phosphate-CMF ones (47 $Lh^{-1}m^{-2}bar^{-1}$). Water flux of all membranes was in agreement with the intercapillary width (narrow intercapillary width implies low water permeability), suggesting that water permeability and intercapillary width of produced functionalized membranes were in the following order: pristine-CMF < carboxylic-CMF < methyl-CMF < phosphate-CMF.

We estimated the NaCl rejection from the different functionalized membranes with a thickness range from 50 μm up to 150 μm using a salt concentration of 0.1 M. All the functionalized nanolaminate membranes were capable of separating NaCl efficiently from water and the salt rejection was maintained as high as 85% for methylated membranes with a thickness of 150 μm for a water flux of 54 $Lm^{-2}h^{-1}bar^{-1}$ (**Figure 3C**).

Membrane performance in the separation of metal ions.

To test the performance of the functionalized nano laminated membranes in separating metal ions from water, we selected four metal species, namely Cd^{2+}, Co^{2+}, Cr^{3+} and Mg^{2+} . where the ionic radius decreases in the order:Cd^{2+} (0.95 Å) > Co^{2+} (0.88 Å)> Mg^{2+} (0.86 Å)> Cr^{3+} (0.75 Å) as shown in **Figure 3D**. The effect of interfiber spacing was investigated adjusting the thickness of functionalized membranes to 100 μm through volume control. The experiment was carried out in dynamic mode by applying 1.0 bar pressure in a dead-end cell. The highest removal percentage was recorded for the phosphorylated nanolaminate membranes with a removal percentage between 70 and 90. This seems in contrast with the packing of the fibers but associated with the negatively charged characters of the functionalizing groups

To prove this hypothesis, we tried to correlate these results with the analyzed ζ-potential and calculated change densities (**Figure S2 and Table S1**) of the created membranes. The phosphate-CMF sample (at pH 5.0) had the lowest ζ-potential, which was followed by the ones of the carboxylic-CMF and pristine-CMF models. Instead, a positive ζ-potential was recorded for methyl-CMF. The phosphate-CMF membrane had the highest charge density (198±2.4 μmole/g) (**Table S1**) and, as a consequence, a more significant number of anchoring sites for capturing the positively charged metal ions. Hence, these findings confirm the adsorption efficiency of the new nanolaminate

membranes[27]. Moreover, the dual behavior makes these membranes unique for the separation of both charged and uncharged impurities in one go.

In the case of methyl-CMF, which showed a positive surface charge, it was impossible to entrap the positively charged metal ions only by electrostatic interactions. In fact, the chelation process, in this case, should be was accompanied by other effects as discussed by Han et al.[2].

Effect of functionalization on the separation of molecular dye and drugs.

To further validate our approach, we assessed the performance of functionalized nanolaminate membranes for efficient nanofiltration by measuring the permeation rate of three micropollutants in a dead-end configuration. We selected, as representative compounds, an organic dye (methyl blue), a psychoactive drug (caffeine), and a conventional medicine (porphyrin), which can hardly be removed from the environment because the methods are scarce and costly. The average size of these micropollutants spans a broad range from 12 Å up to 270 Å. Our measurements revealed that the rejection R ($R=1- C_{permeate}/C_{feed}$) was higher than 90% for the dye and the porphyrin drug, but lower in the case of caffeine. The molecular size of the dye is approximately 1.25 x 0.57 x 0.5 nm (**Figure 3E**); thus, easy blocking of the dye was analyzed for all nanolaminate membranes in dynamic mode.

To disclose the effect of the different functionalizations on the separation of the positively charge dyes, a model wastewater containing the dye was incubated with all nanolaminate membranes. The highest adsorption was obtained with the phosphate-CMF sample, followed by the carboxylic and pristine-CMF membranes. This is in agreement with the trend observed for metal ions and confirms the electrostatic nature of the interaction. The low percentage removal obtained with the methylated nanolaminate membranes is probably due to the unfunctionalized hydroxyls on CMF, which could favorably interact with the dye. In an earlier study[12], freeze-dried cellulose nanocrystals based membranes could remove 98% of crystal violet dye in static mode[12].

Moving to the tests related to the separation of drugs, an effect of intercapillary space of nanolaminate membranes was evaluated with respect to the Stokes radius of the porphyrin and caffeine molecules. The Stokes radii of caffeine and porphyrin are 0.387 nm[28] (Price et al. 1989) and 27 nm[29], respectively. The larger radius of porphyrin compared to the tuned interfiber spacing of membranes makes it

10

impermeable through the capillary; thus, the complete removal of porphyrin was assessed using all nanolaminate membranes. In the case of caffeine, the shorter (2.22 Å) intercapillary spacing holds the drug on the surface. The broader interfiber spacing of the other functionalized membranes rendered the capturing process almost impossible, and thus, very low rejection rates of caffeine were reported (**Figure 3F).**

Figure 3

Molecular dynamics simulations of the CMF-models in water solution.

The computational activity parallel to the experiments was beneficial for explaining further the main characters of the CMF models and their actions. In all of the models, the conformation of the microfibrillated cellulose chains, which were interconnected through highly dynamic networks of hydrogen bonds involving oxygens and hydroxyl groups, were perturbed by the concerted action of the surrounding water molecules and counterions that induced a reorganization of the outer shell of the supramolecular structure. The initial tight packing was loosened, and a few water molecules and ions could migrate between the chains, becoming occasional mediators in the hydrogen-bonding networks. The core of the fibril was, instead, less affected by the perturbations of the surrounding solutions and maintained an almost elongated geometry very close to the starting arrangement. Indeed, the main changes took place at the edges where the glucosyl chains became slightly bent. The degree of bending was mitigated by ion and water penetration. It was observed that besides the reduction of the net charge of the microfibril, the loaded ions weakened the electrostatic repulsion and induced effective, attractive interactions. These were responsible for the moderate conformational rearrangements of the various segments, which determined morphological changes in the microfibril that stabilized the structures. It was found that local variations of the environment (corresponding to localized variations of pH), determined by the presence of different amounts of ions in close contact with the cellulose matrix, could markedly affect its conformation and change the whole charging equilibrium of the system[30].

Furthermore, an inspection of the length of the side chains (functionalizing groups) revealed that in the methylated and phosphorylated CMFs these had the tendency to adopt more elongated arrangements than in the carboxylate and pristine MFC models, where they could extend only to approximately 2.5 Å (**Figure 4 a, b**) toward the

11

solution. Indeed, methyl and phosphate moieties could reach at most 4.8 and 5.7 Å (**Figure 4 c, d**), respectively, were more flexible and could be rearranged more appropriately in response to the surrounding environment without inducing remarkable reorganizations of the backbone of the main chains (mainly, the glucosyl rings). The length of these grafted functional groups is also discussed previously and reported in **Table S3,** and these computational modulations are in agreement with theoretical findings.

Figure 4

These characteristics, together with the charged nature of the functionalizing moieties, had an impact on the packing arrangements and water content of the fibers. The analysis of the first solvation shell of the wet fibers showed that the hydration of the phosphorylated CMF is greater than that of the other models (about 30% greater than the carboxylate CMF one). This is due not only to the length of the side chains but also to the presence of the charge balancing counterions that are themselves surrounded by water molecules. Evidence of this behavior is provided by the analysis of the pair distribution functions displayed in **Figure 5**, which indicate that the ions are well coordinated to both carboxyl and phosphate oxygens. Inspection of their dynamics also revealed that they preserved their locations close to the headgroups. This is also evident from the comparison of the atom-atom distribution functions (PDF) of the dried models **Figure 6**.

As is easily seen, ion-ion PDFs display superimposed sharp peaks at approximately 3.2-3.8 Å and a flat region between the first and the second peaks which confirms the stability of the ions on the CMF surface at close distances, primarily determined by the location of the capturing groups of the chains, in all cases. It was also observed that the drying process drove the ions close to the phosphate groups (**Figure 6**). This could be ascribed to the length of the chain because it was not the case for the carboxyl groups.

Figure 5

Figure 6

12

Computational modeling of the packing arrangements

An idea of the packing arrangements of the various types of functionalized CMF membranes could be obtained through the simulation of the drying process and the examination of the stabilized dried models. These were obtained by removing all the water molecules far from the fibers and by optimizing the CMF packing arrangements through the re-equilibration of simulation boxes and molecular configurations. Essentially, the systems were re-equilibrated in the new environment, where all the counterions and only a few water molecules were present, through a series of MD-NPT runs long enough to obtain the correct system density. Only the water molecules tightly connected to the CMF chains were retained because they were basically entrapped in the fibers. This strategy was useful to estimate possible interlayer spacing, channels, and cavities. Even though it was not straightforward, it was helpful to visually compare the degree of envelopment by replicating the final configurations in all directions and looking for gaps and water sites (**Figure 7**)

Figure 7

The size of these regions depended on the morphology of the systems, which presented variable arrangements along the chains and different degrees of functionalization. The size of these regions was regulated not only by the elongation of the various side chains but also by the trapped ions and water molecules. It is worth pointing out that the orange areas visible in **Figure 5** identify both water and empty regions without distinction. Visual examination of the three cases suggests that the packing differences are subtle and cannot be quantified accurately due to the great variety of interactions. However, more interconnections can be obtained when CMF is functionalized with carboxyls; phosphorylation seems to induce a slight separation of the fibers, whereas methylation keeps the fibers more compact but quite separated with more empty regions. The size of these gaps are very small and cannot be compared directly with the experimental findings. A tentative estimate of these cavities revealed that the sizes range was between 3 and 7 Å for all the models.

Conclusions

We have prepared novel CMF nanolaminate membranes with superior properties and shown that a tuned functionalization of microfibrillated cellulose can efficiently control the interlayer spacing and enhance the sieving performance of the membranes. The functionalized membranes demonstrated remarkable performance towards water purification and desalination compared to the current state-of-the-art. Our results suggest that the packing of fibers has a direct influence on the resulted inter-layer spacing and can be modulated on purpose to design more selective scavengers. The interfiber spacing can also be changed on purpose and adapted to the surrounding environment. We believe that our strategy is very promising and paves the way for the preparation of membranes with tunable sieving . The control of the surface chemistry of microfibrillated 2D materials allows further exploration of the nanofluidic phenomena inside nanolaminate membranes at fundamental and practical levels for water purification.

Acknowledgments

Conflict of Interest

No conflict of interest was recorded

References

1. H. Hoga, M. Nogi, N. Komoda, T. T. Nge, T. Sugahara, K. Suganuma, Uniformly connected conductive networks on cellulose nanofiber paper for transparent paper electronics, *NPG Asia Mat.,* 2014, **2**, 93.

2. Y. Han, Z. Xu, C. Gao, Ultrathin grapheme nanofiltration membranes for water purification *Adv. Funct. Mater.*, 2013, **23**, 3693-3700.

3. Z. Karim, S. Claudpierre, M. Grahn, K. Oksman, A. P. Mathew, Nanocellulose based functional membranes for water cleaning: Tailoring of mechanical properties, porosity and metal ion capture. *J. Membrane Sci.*, 2016, **514**, 418-428.

4. Z. Karim, A. Svedberg, K. Y. Lee, M. J. Khan, Processing-structure-property correlation understanding of microfibrillated cellulose based dimensional structures for ferric ions removal. 2019, *Scientific Report.*, **9**, 10277.

5. F. M. Sukuma, P. Z. Culfaz-Emecen, Cellulose membranes for organic solvent nanofiltration, *J. Memb. Sci.*, 2018, **545**, 329-336.

6. L. Bai, U. Liu, N. Bossa, A. Ding, N. Ren, L. H. Guibai, M. R. Liang, Wiesner. Incorporation of cellulose nanocrystals (CNCs) into the polyamide layer of thin-film composite (TFC) nanofiltration membranes for enhanced separation performance and antifouling properties. *Environ. Sci. Technol.*, 2018. **52**, 11178-11187.

7. A. W. Carpenter, C. F. de Lannoy, M. R. Wiesner, Cellulose nanomaterials in water treatment technologies. *Environ. Sci. Technol.*, 2015, **49**, 5277-5287.

8. P. Xu, J. E. Drewes, T. U. Kim, C. Bellona, G. Amy, Effect of membranes fouling in transport of organic contaminants in NF/RO membranes applications. *J. Memb. Sci.*, 2006, **279**, 165-175.

9. A. S. Bolisetty, A. M. Peydayesh, R. Mezzenga, Sustainable technologies for water purification from heavy metals: review and analysis. *Chem Soci. Rev.*, 2019, **48**, 463-487.

10. C. Zhu, S. Monti, A. P. Mathew, Evaluation of nanocellulose interactions with water pollutants using nanocellulose colloidal probes and molecular dynamic simulations. *ACS Nano,* 2020, **229**, 115510..

11. H. Ma, C. Burger, B. S. Hsiao, B. Chu, Fabrication and characterization of cellulose nanofiber based thin-film nanofibrous composite membranes. *J. Memb. Sci*., 2014, **454**, 271-282.

12. Z. Karim, A. P. Mathew, J. MouzonK. Oksman, Nanoporous membranes with cellulose nanocrystals as functional entity in chitosan: Removal of dyes from water. *Carboh. Poly*., 2014, **112**: 668-676.

13. M Jiao, Y. Yao, C. Chen, B. Jiang, G. Pastel, Z. Lin, Q. Wu, M. Cui, S. He, L. Hu. Highly efficient water treatment via a wood-based and reusable filter. *ACS Mat. Let*., 2020, **2**, 430-437.

14. A. Celebioglu, F. Topuz, Z. I. Yildiz, T. Uyar, Efficient removal of polycyclic aromatic hydrocarbons and heavy metals from water by electrospun nanofibrous polycyclodextrin membranes. *ACS Omega*, 2019. **4**, 7850-7860.

15. J. Li, C. Si, H. Zhao, Q. Meng, B. Chang, M. Li, H. Liu, Dyes adsorption behavior of Fe3O4 nanoparticles functionalized polyoxometalate hybrid. *Molecules,* 2019, **24**, 3128..

16. Y. Habibi, Key Advances in the chemical modification of nanocelluloses. *Chem. Soc. Rev*., 2014, **43**, 1519-1542.

17. Z. Karim, S. Afrin, Q. Husian R., Danish, Necessity of enzymatic hydrolysis for production and functionalization of nanocelluloses. *Crit. Rev. Biotechnol*., 2017, **37**, 355-370.

18. P. Orsolini, B. Michen, A. Huch, P., Tingaut, W. R. Caseri, T. Zimmermann, Characerization of pores in dense nanopaper and nanofibrillated cellulose membranes: A critical assessment of established methods. *ACS Appl. Mater. Inter*., 2015, **46**, 25884–25897.

19. A. Serra, I. Gonzalez, H. Oliver-Ortega, O. Tarres, M. Delgado-Aguilar, P. Mutje, Reducing the amount of catalyst in TEMPO-oxidized cellulose nanofibers: Effect on properties and cost. *Polymer,* 2017, **9**, 557-571.

20. M. Bozic, P. Liu, A. P. Mathew, V. Kokol, Enzymatic phosphorylation of cellulose nanofibers to new highly-ions adsorbing, flame-retardant and hydroxyapatite-growth induced natural nanoparticles. *Cellulose,* 2014, **21**, 2713-2726.

21. M. Ghanadpour, B. Wicklein, F. Carosio, L. Wågberg, All-natural and highly flam-resistant freeze-cast foams based on phosphorylated cellulose nanofibrils. *Nanoscale*, 2018, **10**, 4085..

22. C. Zhu, S. Monti, A. P. Mathew, Cellulose nanofiber–graphene oxide biohybrids: disclosing the self-assembly and copper-ion adsorption using advanced microscopy and ReaxFF simulations. *ACS Nano, 2018,* **127**, 7028-7038.

23. M. Henriksson, L. A. Berglund, P. Isaksson, T. Lindstrom, T., Nishino, Cellulose nanopaper structures of high toughness, *Biomacromolecules*, 2008, **9**, 1579-1585.

24. J. Abraham, K. S. Vasu, C. D. Williams, K. Gopinadhan, Y. Su, C. T. Cherian, J. Dix, E. Prestat, S. J. Haigh, I. V. Grigorieve, P. Carbone, A. K. Geim, R. R. Nair, Tunable sieving of ions using graphene oxide membranes. *Nat. Nanotechnol.*, 2017, **12**, 546–550.

25. Z. Karim, M. Hakalahti, T., Tammelin, A. P. Mathew, K. Oksman, Effect of in situ TEMPO surface functionalization of nanocellulose membranes in the adsorption of metal ions form aqueous solution, *RSC Advances,* 2017, **7**, 5232-5241.

26. Z. Karim, M. Grahn, K. Oksman, A. P. Mathew, High flux affinity membranes based on cellulose nanocompoite for removal of heavy metal ions from industrial effluent *RCS Advance,* 2016, **6**, 20644-20653.

27. A. Mautner, H. A. Maple, T. Kobkeatthawin, V. Kokol, Z. Karim, K. Li, A. Bismark, Phosphorylated nanocellulose papers for copper adsorption from aqueous solutions. *Int. J. Environ. Sci. Technol.*, 2016, **13**, 1861-1872.

28. W. E. Price, Tracer caffeine diffusion in aqueous solutions at 298 K. The effect of caffeine self-association. *J. Chem. Soc., Faraday Trans. 1: Phy. Chem. Conden. Phases*, 1989, **85**, 415-419.

29. X. Gong, T. Milic, C. James, D. Batteas, C. M. Drain, Preparation and Characterization of Porphyrin Nanoparticles, *J. Am. Chem. Soc.*, 2012, **124**, 14290-14291.

30. V. S. Rathee, H. Sidky, B. J. Sikora, J. K. Whitmer, Role of associative charging in the entropy–energy balance of polyelectrolyte complexes. *J. Am. Chem. Soc.*, 2018, **140**, 15319–15328.

Figure titles/legends

Figure 1: SEM images of arrested CMF and fabricated 2D nanolaminated membrane. **(A)**, SEM image of CMF after freeze-drying (arrest form). **(B)**, Produced 2D membrane like framework using vacuum-filtration. **(C)**, surface morphology of produced membrane and **(D)**, cross-morphology of membrane indicates laminated layering in horizontal direction. Four nanolaminate membranes having modified CMF (Supplementary **Figure S1A, B, C, D**) were produced as mentioned in Supplementary **Figure S1E and S2**.

Figure 2: Characterization of produced nano-laminated functionalized membranes. **(A)** XRD spectra of pristine and functionalized CMF membranes. **(B)** The contact angle of all the functionalized membranes. Phosphate-CMF had the lowest contact angle (highly hydrophilic). **(C)**Swelling % of functionalized membranes was also analyzed, the highest swelling was observed for pristine-CMF, and the methylated-CMF membranes showed slight compact arrangements. (D) Evolution of inter-fibril space of pristine-CMF and functionalized CMF membranes when immersed in water. A detailed analysis of all the experiments is included in the supplementary file.

Figure 3: Performance of membranes: **(A)** permeation rate of phosphate-CMF membranes for Na^+, K^+ and Li^+ with increasing ionic strength. **(B)** All three ions were also targeted using methyl-CMF membranes. **(C)** water permeability of all fabricated membranes and NaCl rejection of phosphate and methyl-CMF membranes. **(D)** polluted water from an industrial site having four metal ions (Cd^{2+}, Co^{2+}, Cr^{3+} and Mg^{2+}) were separated using fabricated functionalized membranes. **(E)** Polluted water model containing methylene blue. Adsorption and rejection rate were calculated as mentioned in the **Supporting file**. **(F)** Porphyrin and caffeine were selected to

evaluate the separation performance of the produced functionalized membranes. Solid lines denote removal capacity (mg/g) and dotted lines denote removal (%) **(D)**. In **(E)** green, blue, black and red columns indicate phosphate, carboxylic, methyl and pristine-MFC membranes, respectively.
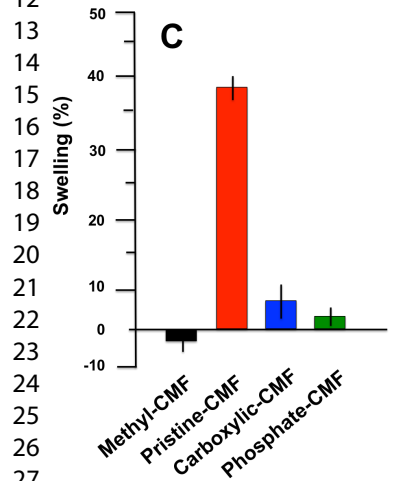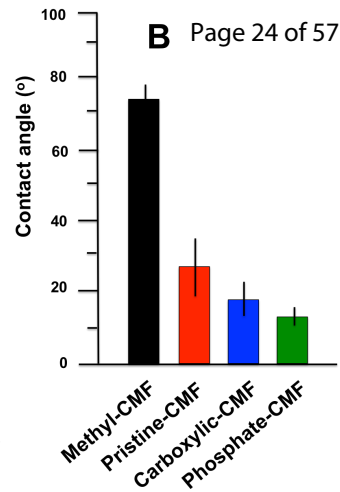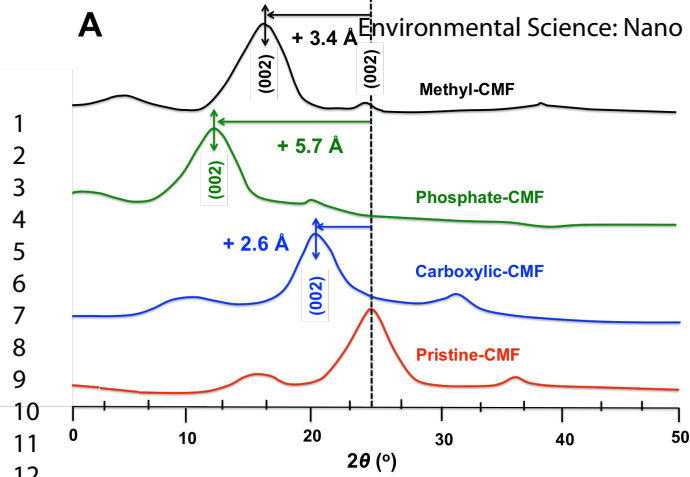
Figure 4. Molecular structures representing the sidechains in the pristine (a) and functionalized-CMF (b, c and d) models. The sidechains and the corresponding glucosyl units are rendered with sticks, whereas the rest of the cellulose chains are depicted through wires (oxygen, carbon, phosphate, and hydrogen atoms are red, gray, orange and white, respectively). A few water molecules in the first shell around the cellulose fiber are also displayed.

Figure 5. Atom-Atom distribution functions. **a.** O-Na^+ (blue line), Na^+–Na^+ (red line) obtained from the last portions of the production trajectory of carboxylated-CMF, **b.** P-O(water); **c.** O-Ca^{2+} (blue line), P-Ca^{2+} (orange line), Ca^{2+}-Ca^{2+} (red line), obtained from the last portions of the production trajectory of phosphorylated-CMF.

Figure 6. Atom-Atom distribution functions. O-Ca^{2+} (blue line with circles), P-Ca^{2+} (orange solid line with circles), Ca^{2+}-Ca^{2+} (red line with circles), obtained from the last portions of the production trajectory of phosphorylated-CMF in solution and of the corresponding dried model (solid lines).
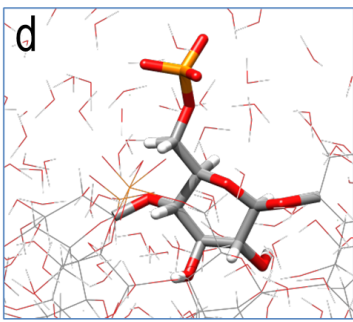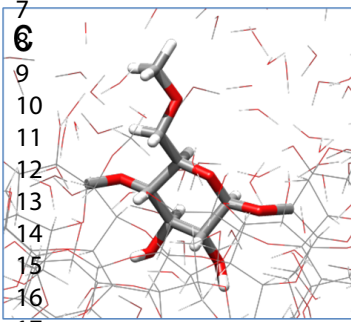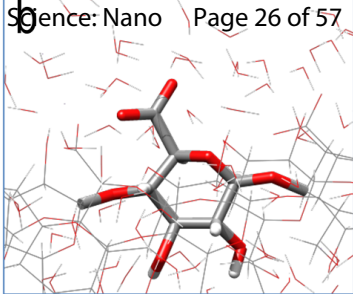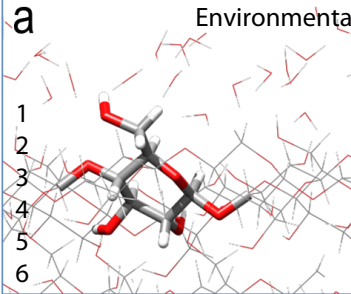
Figure 7. Packing of the dried fibrils models. The CMF fibers are rendered through the solvent-accessible surface, whereas water, channels, and cavities are displayed as orange areas. The numbers 1, 2, 3, 4 represent the replicated models, whereas the axes indicate the directions of the replication. Pristine-CMF is displayed in **Figure S14** of the supporting material.

a X(CMF)-Na$^+$ distance (Å)
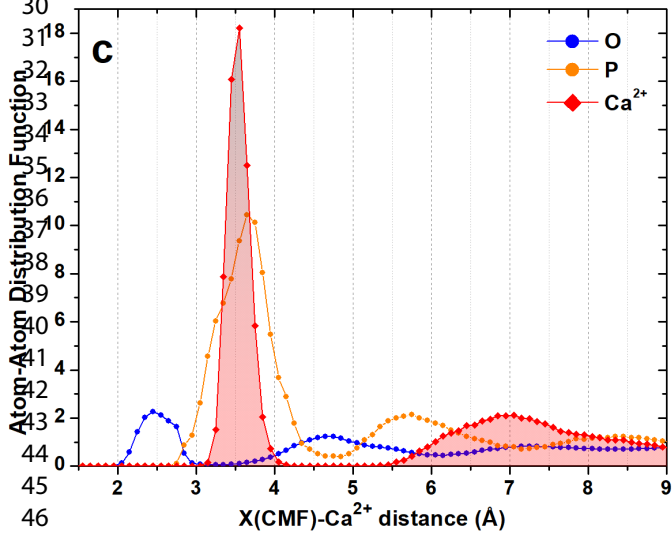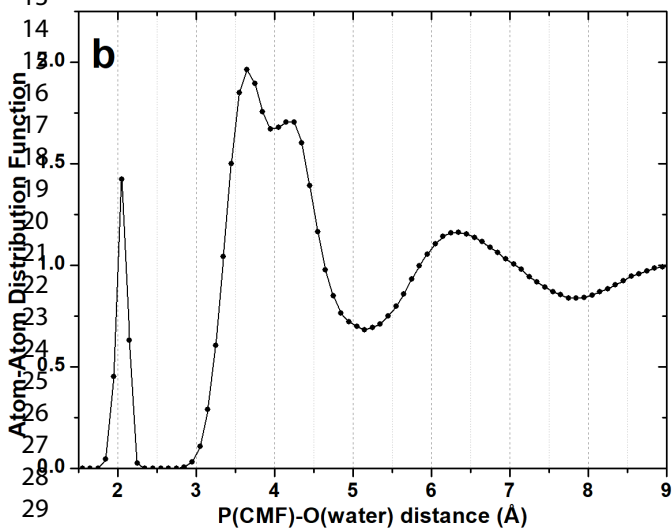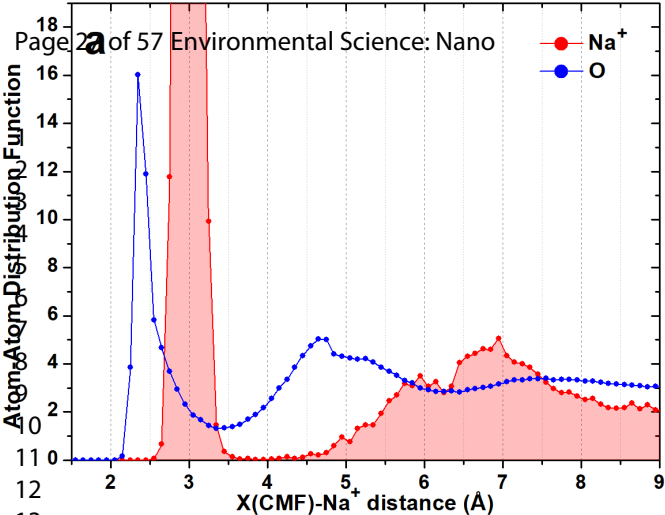
Atom-Atom Distribution Function

Legend: Na$^+$, O

b P(CMF)-O(water) distance (Å)

Atom-Atom Distribution Function

c X(CMF)-Ca^{2+} distance (Å)

Atom-Atom Distribution Function

Legend: O, P, Ca^{2+}

Carboxylic-CMF   **Phosphate-CMF**   **Methyl-CMF**
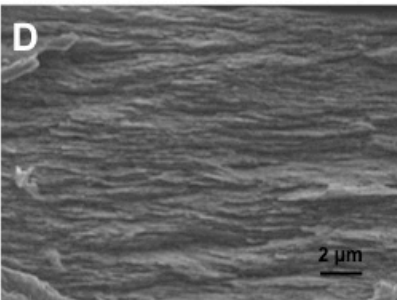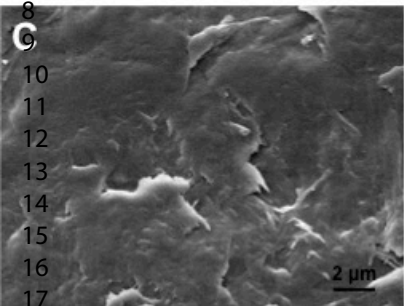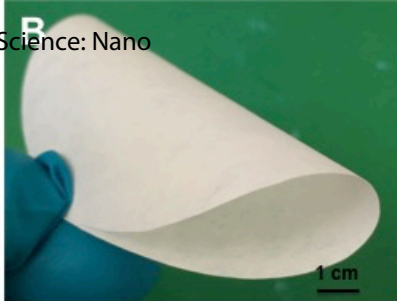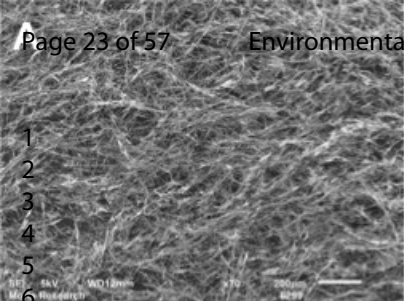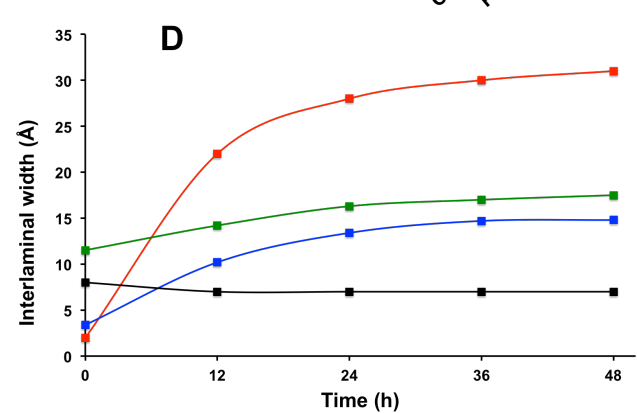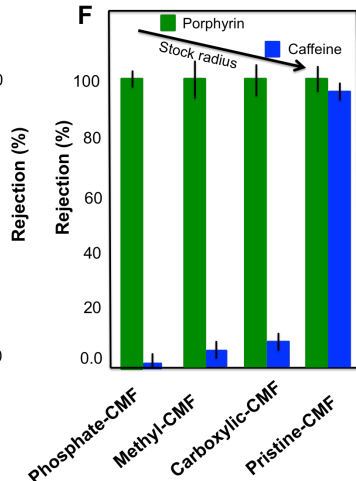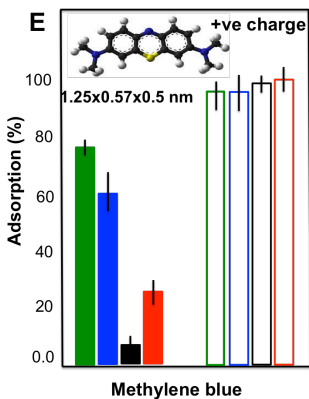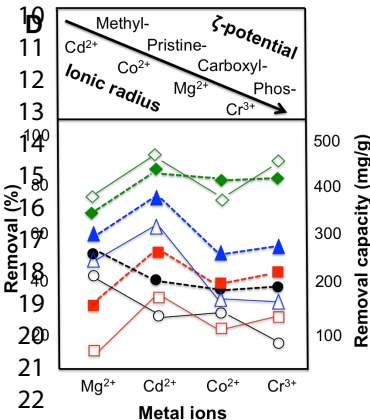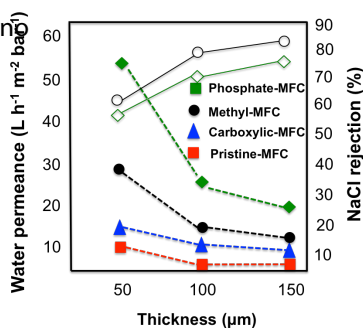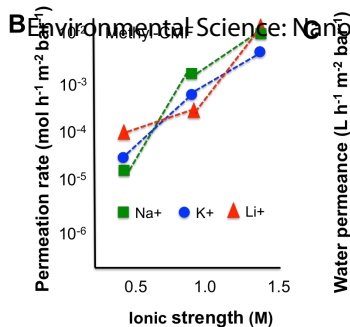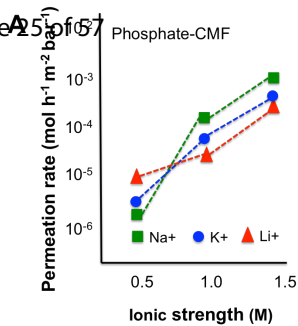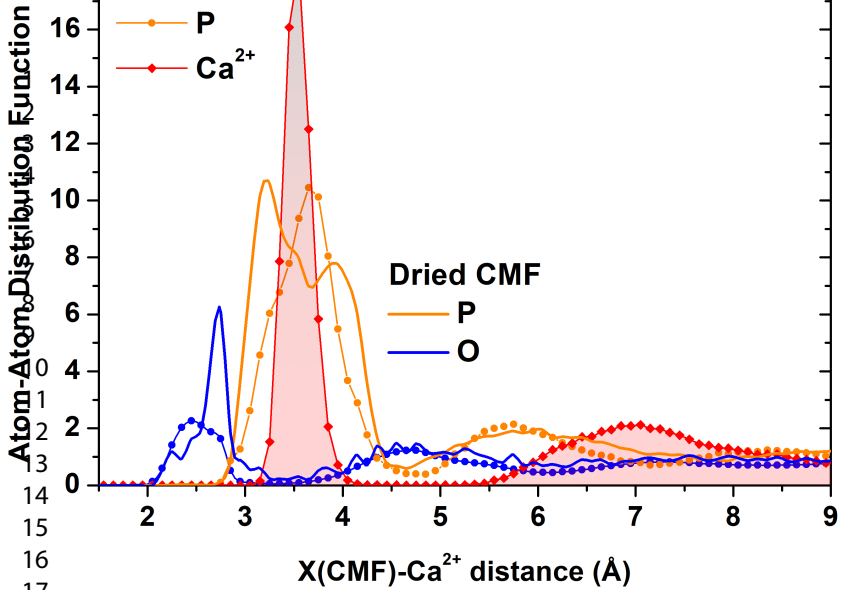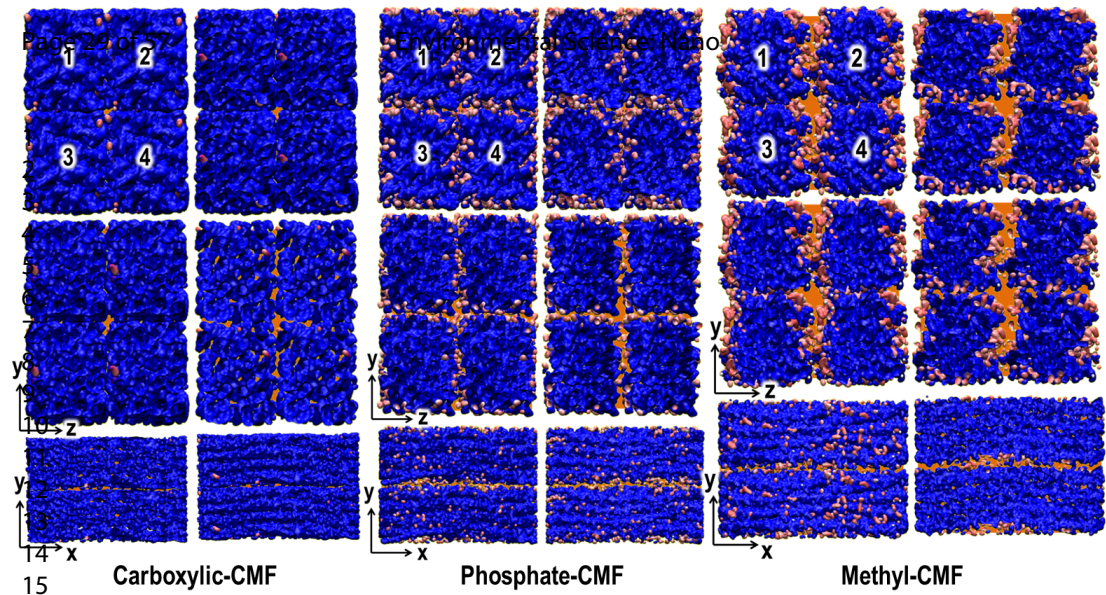
Supplementary materials

Enhanced sieving of cellulosic microfibers membranes via tuning of interlayer spacing

Zoheb Karim[1,2],[*] Susanna Monti[3*], Giovanni Barcaro[4], Anna Svedberg[1], Mohd Ayub Ansari[5], Sadaf Afrin[6]

[1]MoRe Research Örnsköldsvik AB, Box 70, SE-89122, Örnsköldsvik, Sweden

[2]Institute of Architecture and Civil Engineering, South Ural State University, Chelyabinsk, 454080, Russia

[3]CNR-ICCOM– Institute of Chemistry of Organometallic Compounds, via Moruzzi 1, 56124 Pisa, Italy

[4]CNR-IPCF–Institute for Chemical and Physical Processes, via Moruzzi 1, 56124 Pisa, Italy

[5]Department of Chemistry, Bipin Bihari College, 284001, Jhansi, India

[6]Department of Chemistry, Faculty of Chemical Sciences, Aligarh Muslim University, Aligarh 202002, India

Corresponding authors: Z.K (zoheb.karim@gmail.com)

S.M (sapeptides@gmail.com)

1
2
3
4
5
6
7
8
9
10
11
12
13
14
15
16
17
18
19
20
21
22
23
24
25
26
27
28
29
30
31
32
33
34
35
36
37
38
39
40
41
42
43
44
45
46
47
48
49
50
51
52
53
54
55
56
57
58
59
60

Table of content:

S.No	Sections		
1.	**Materials**		
2.	**Functionalization of cellulose microfibers (CMF)**		
	2.1.	TEMPO oxidation	
	2.2.	Phosphorylation	
	2.3.	Methylation	
3.	**Fabrication of nanolamnated membranes**		
4.	**Characterization of nanolaminated membranes**		
	4.1.	Scanning Electron Microscopy (SEM)	
	4.2.	Surface ζ-potential measurement	
	4.3.	Quantitative analysis of functional groups	
		4.3.1	Carboxylic
		4.3.2.	Phosphate
		4.3.3.	Methyl
	4.4.	Infrared spectroscopy	
	4.5.	^{13}C CP MAS and ^{31}P MAS NMR spectroscopy	
	4.6.	XRD analysis	
	4.7.	XPS analysis of functionalized CMF	
	4.8.	Water permeability of nanolaminated membranes	
	4.9.	BET measurement	
	4.10.	Mechanical properties and air permeance	
5.	**Nanolaminated membranes separation performance**		
	5.1.	Ions permeation rate	
	5.2.	Membrane performance for removal of metal ions, dye and drugs	
6.	**Model building and simulation details**		
7.	**References**		

1. Materials:

Cellulose microfibers (CMF) (Exilva P 01-V) was supplied by Borregaard AB (Sarpsborg, Norway). The charge density of CMF was 28.54±4.09 μmole/g and dry weight concentration was 9.3 wt%. Enzyme hexokinase was purchase from Novozymes, USA. 2,2,6,6-tetramethyl-1-piperidinyloxy (TEMPO) and all other chemicals used in this study were purchased from Sigma Aldrich, USA. Chemicals (analytical grade) were used without any further purification.

2. Functionalization of Cellulose microfibers (CMF): CMF were functionalized using chemicals and enzyme hexokinase and denoted functional groups were introduced on the surface of CMF.

2.1. *TEMPO oxidation:* CMF suspension was oxidized as discussed by Serra et al.[1].. In a typical experiment, 15 g of CMF were dispersed in distilled water containing previously dissolved TEMPO (0.0156 g per g of MFC) and NaBr (0.1 g per g of CMF). The mixture was stirred for 15 min in order to assure good dispersion of all the substances. After mix, a 3.0, 6.0 and 10.0 ml of 10 wt% NaClO solution was added to the slurry. The pH was kept at 10 by addition of 0.5 M NaOH solution. The oxidized CMF were then filtered and washed with Milli-Q water and stored for further use.

2.2. *Phosphorylation:* Surface modification of CMF (1 wt%) using enzyme hexokinase was performed as discussed by Bozic et al[2] Briefly, reaction proceeds in 1 wt% of CMF in phosphate buffer (pH 7.6) in the presence of a 50 mM ATP, 50, 100 and 200 mM of $MgCl_2$ and 35 U ml^{-1} of enzyme for 24 h at 30 °C.

2.3. *Methylation:* CMF (1 wt%) was mercerized using 60 mL NaOH solution (50% m/v) for 1 h at room temperature. The excess NaOH was removed by filtration and acetone (27.0 mL) was added as a solvent. Dimethyl sulfide (DMS) (9.0 mL) was added drop-wise and the reaction was carried out at 50 °C. After 1 h of reaction, the system was filtered and fresh reagents were added (acetone and DMS), maintaining the same previous proportions. At the end, the sample was neutralized using acetic acid (10% v/v), filtered, and washed with acetone (three times with 90 mL) and finally dried in an oven at 50 °C for 6 h. The synthesis process was adapted from Vieira et al. (2007).
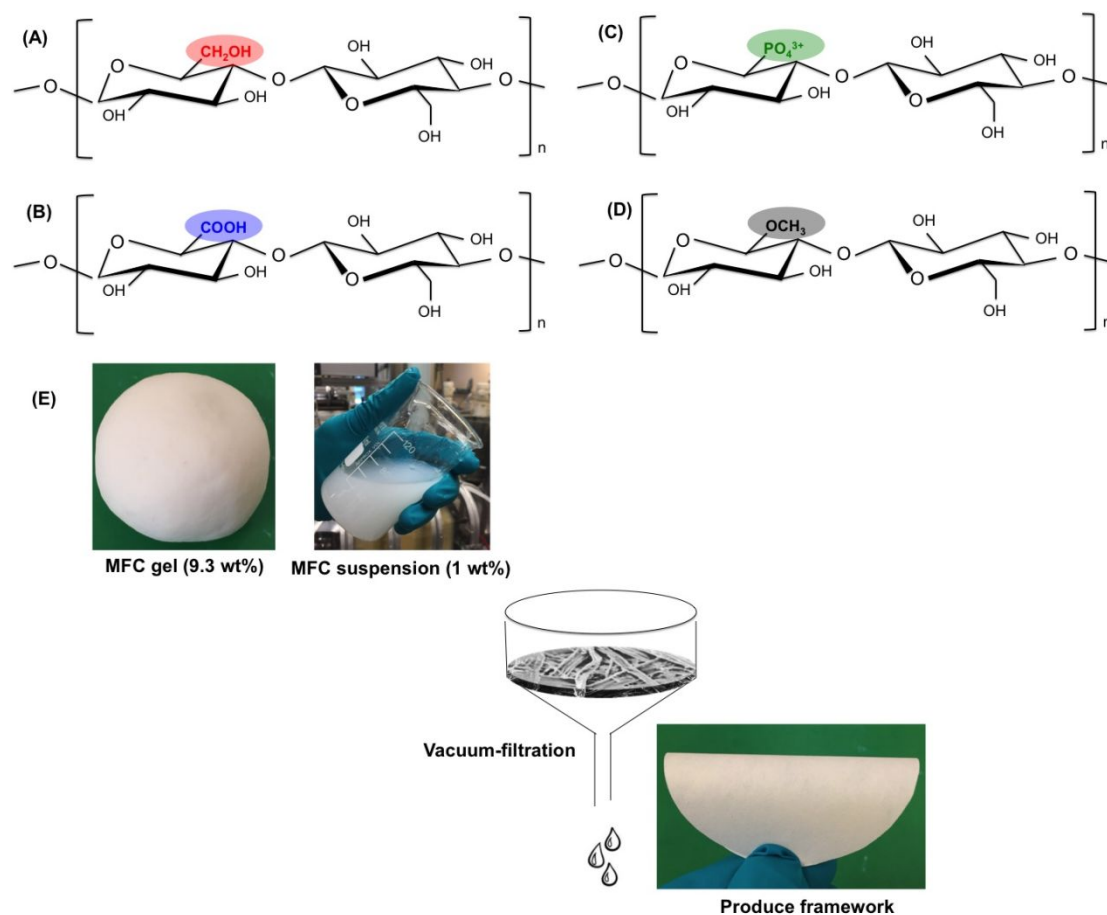
Figure S1: Introduction of functional groups on C6 carbon of cellulose monomer after functionalization of CMF. **A**, pristine-CMF having hydroxyl (-OH) group on C6. **B**, TEMPO functionalization of CMF introduced carboxylic (-COOH) group on CMF. **C**, phosphorylation of CMF using enzyme hexokinase and introduce phosphate (PO_4^{3-}) group on CMF. **D**, Methylation of CMF and introduced methyl hydrophobic group (CH_3). **E**, Nanolaminate membranes were produced using very simple and scalable technique, vacuum-filtration. The 1 wt% of CMF suspension (150 ml) was filtered using funnel. It is worth mentioning that except methyl groups all three groups are hydrophilic in nature.

3. Fabrication of nanolamimate membranes:

2D membranes were fabricated using vacuum filtration. Total 150 ml of pristine and functionalized CMF suspensions (1wt % each) was filtered using a Buchner funnel setup (600 ml of volume capacity). After the draining off of the water, the filtered frameworks were removed from the Buchner funnel and dried at room temperature

for 48 h and whatman papers were replaced after each 10 h for fast drying. Produced frameworks (12.5 cm in diameter) were denoted as pristine-CMF, carboxylic-CMF, phosphate-CMF and methyl-CMF nanolaminate membranes with respect to their introduced functional groups (**Figure S1E**).

4. Characterization of membranes:

4.1. Scanning Electron Microscopy (SEM):

The membranes sputter coated with tungsten were observed in the SEM (MAGELLAN 400, SEM, FEI Company) at an acceleration voltage of 3 kV to understand the morphology and nanostructure.
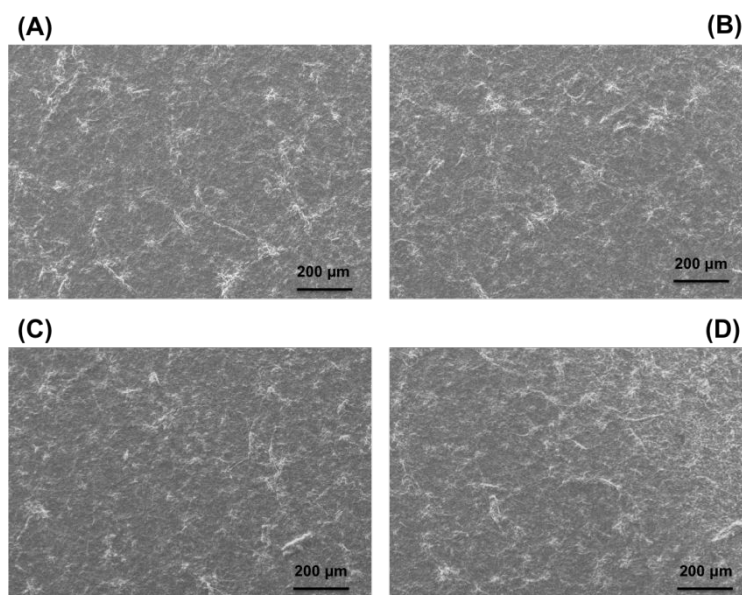

Figure S2: SEM images of fabricated membranes. SEM images of fabricated membranes were captures at 3 kV using low-resolution microscopy. SEM images of pristine-CMF, phosphorylated-CMF, carboxylic-CMF and methyl-CMF membranes were represented in image (a), (b), (c) and (d), respectively.

4.2. Surface ζ-potential measurement:

Mutek SZP 06, MUTEK (Sweden) device was used for the measurement of ζ-potential of suspensions (pristine-CMF, TEMPO-oxidized-CMF, phosphorylated-CMF and methyl-CMF). The ζ-potential of suspensions was measured respect to pH

ranges (2 to 12) as shown in **Figure S3.** Furthermore, quantitative measurement of functional groups density is reported in **Table S1**.
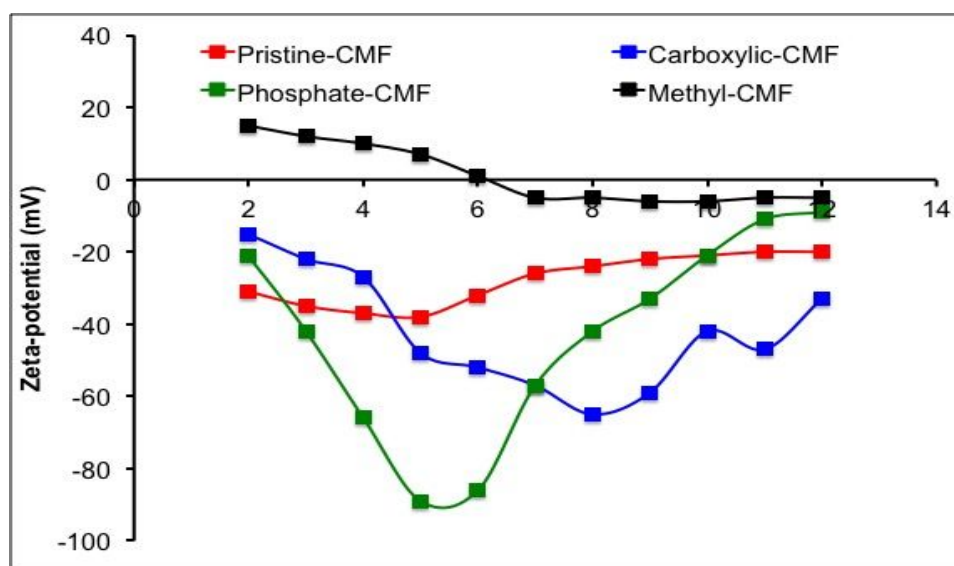
Figure S3: ζ-potential of pristine and functionalized CMF suspensions. 500 ml of suspension was used for the measurements. Reported data was in an average of three independent measurements.

4.3. Quantitative analysis of functional groups (functional group density):

4.3.1. *Carboxylic:* Conductometric titration was done with a three-necked round-bottom flask as discussed by Junka et al.[3] In detail, the prescribed amount of CMF was diluted, 2 ml of 0.1M NaOH was added, and the dispersion was mixed for 1 h at 400 rpm at a total volume of 495 ml. after mixing, the ionic strength of the dispersion was adjusted with NaCl (5 ml of 10 mM NaCl) and samples were titrated with 0.1 M HCl using automatic titrator. CO_2 was removed by bubbling N_2 gas before and during titration. The total amount of functional groups in the sample was determined from the titration curve (conductivity as a function of the amount of H^+ added)[4].

4.3.2. *Phosphate:* Furthermore, the concentration of phosphate groups on CMF was determined using Inductive Coupled Plasma Atomic Emission Spectroscopy (ICP-OES, Optima 2000 DV, Perkin Elmer, USA) after the mineralization of native and phosphorylated-CMF samples in boiling HNO_3 and H_2O_2. In order to ensure the acidic form of phosphate groups, samples were first washed several times with diluted HCL to pH 4.0 and then mineralized[5].

4.3.3. *Methyl:* The determination of methyl groups content was made through the method discussed by Chen[6] with some modifications as discussed by Viera et al.[7]

**Table S1:** Quantitative analysis of functional group density

Types of CMF	Charge density (µmole/g)
Pristine-CMF	28.54±4.1
Carboxylic-CMF	41.52±2.5
Phosphate-CMF	198±2.4
Methyl-CMF	12.21±3.1

4.4. Infrared spectroscopy: Varian 670- IR FTIR spectrometer was used for the measurement of all surface modifications and interaction within produced frameworks. The used spectrometer was equipped with an attenuated total reflection (ATR) detection device. All samples were scanned in the spectral region of 500-4000 cm^{-1}.

In order to determine the functionalization of cellulosic microfibers, the ATR-FTIR spectroscopy was performed as shown in **Figure S4**. Pristine-CMF has similar FTIR spectra as reported for cellulose nanofibers and cellulose nanocrystals[8,9], the broad band centered at ca 3500 cm^{-1} was related to O-H stretching vibration. The band at 3100 cm^{-1} and 1431 cm^{-1} were characteristic of C-H stretching and bending of CH_2 groups, respectively, where the peaks at 1160 cm^{-1} and 1070 cm^{-1} were typical to the saccharide structure as mentioned and summarized in our previous article[8] for cellulose nanocrystals. Potentiometric titration was performed further to calculate the charge density of hydroxyl groups (**Table S1**) on pristine-CMF and it was to 28.54±4.1 µmole/g [4].

The peak at 1605 cm^{-1} attributed to –COONa due to the C=O stretching of carboxyl groups[10] in the spectra of TEMPO oxidized CMF based membranes. Furthermore, the effect of increased NaClO volume (3 to 10 ml) on functionalization was checked (**Figure S5**). The decrease peaks with respect to increase in the volume of NaClO was detected (**Figure S5**). The charge density of carboxylic group (-COO) was further calculated as reported in method section, decrease in chage density of carboxylic groups from 41.52±2.5 to 28.11±2.1µmole/g was detected as reported in **Table S2**.

The change in peak at 1210 cm^{-1} and 930 cm^{-1} assigned the phosphorylation of pristine-CMF which represents the P=O and P-OH vibration mode, respectively (**Figure S3**)[2,11]. The increase in the absorbance of the peaks at 1645 cm^{-1} (i.e. deformation vibration of water molecules) also suggests incorporation new hydroxyl groups by phosphorylation with increase water uptake. Effect of MgCl$_2$ concentration on the phosphorylation was detected using ATR-FTIR and potentiometric titration experiments. As shown in **Figure S4**, decrease in peak intensity with increased concentration of MgCl$_2$ (50 to 200 mM) was detected. In parallel, decrease in the carboxylic charge density was also recorded in titration experiment (**Table S2**). In has been presorted in the previous published article that high concentration of MgCl$_2$ inhibit the activity of hexokinase enzyme[2].
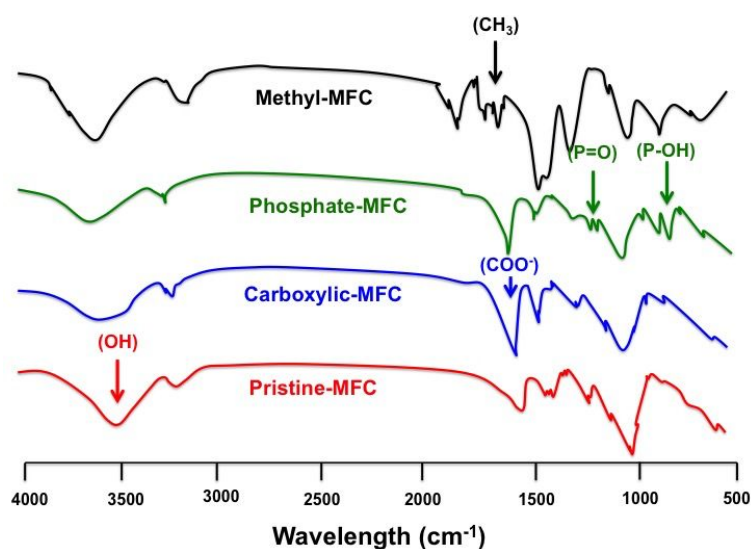
Figure S4: ATR-FTIR analysis of functionalized CMF based frameworks. Introduction of various functional groups were shown by multiple peaks
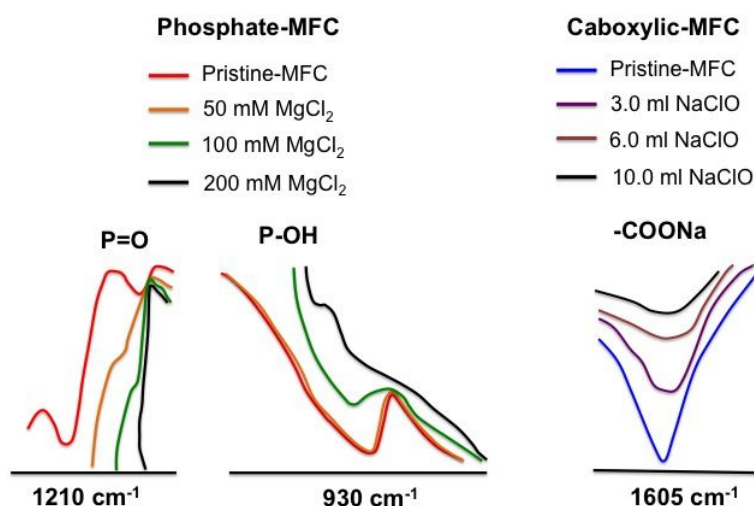
Figure S5: ATR-FTIR analysis of functionalized CMFs (phosphate-CMF and carboxylic-CMF). Change in the intensity by adding $MgCl_2$ (50-200 mM) has been shown here, with a high concentration of $MgCl_2$, peaks at 1210 cm^{-1}, and 930 cm^{-1} vanished. In the case of carboxylic-MFC, peak at 1605 cm^{-1} is shown respect to the various volumes of NaClO. The intensity of peaks is decreased by increasing the concentration of NaClO.

Table S2: Quantitative analysis of functional group density of phosphate-CMF and carboxylic-CMF

| Types of CMF	Variation in chemicals	Charge density (µmole/g)
Carboxylic-MFC	3.0 ml NaClO	41.52±2.5
	6.0 ml NaClO	32.34±1.6
	10.0 ml NaClO	28.11±2.1
Phosphate-CMF	50 mM $MgCl_2$	198±2.4
	100 mM $MgCl_2$	120±4.2
	200 mM $MgCl_2$	80±2.1

Methylation of microfibrillated cellulose was performed using chemicals. Main difference between pristine-CMF and methyl-CMF is the decrease in the intensity and change in the profile for the 3400 cm^{-1} band attributed to the stretching of the O-H bond (hydroxyl) due to partial substitution of hydrogen group during methylation of CMF. Furthermore, an increase is observed for the bands around 3200 cm^{-1} assigned to the C-H stretching due to the presence of the CH and CH_2 groups of cellulose and CH_3 of methyl-CMF. Methyl-CMF spectra usually present bands at 1460, 1380, 1320 and 950 cm^{-1} attributed to C-H stretching of CH_2 and CH_3 (**Figure S4**)[12]. The change in the profile of the band assigned to the stretching of the bond O−H and the region assigned to stretch C−H confirms the efficiency of the methylation process.

4.5. ^{13}C CP MAS and ^{31}P MAS NMR spectroscopy:

The ^{13}C CP/MAS NMR spectra were recorded at 295±1 K in a Bruker Avance III AQS 400 SB instrument operating at 9.4 T for pristine and phosphate-CMF. The MAS rate was 10 kHz and a double air bearing probe and zirconium oxide rotor were

used. Spectra were acquired with a CP pulse sequence using a 2.95 μs proton 90° pulse, a 800 μs contact pulse, and a 2.5 s delay between repetitions. Glycine was used for the Hartmann-Hahn procedure. The chemical shift was calibrated to the TMS $(CH_3)_4$ Si scale by assigning the data point of maximum intensity in the α-glycine carbonyl signal to a shift of 176.03 ppm. For each sample, a total of 4096 or 16384 transients were recorded, resulting in an acquisition time of approximately 3 or 12 h, respectively[2].

The ^{31}P MAS NMR spectra were recorded in a Bruker Avance instrument using a MAS rate of 10 kHz and a 4 mm probe as reported by Ghanadpour et al.[13]. Data were acquired using a contact time of 5 ms of a 90° pulse with a 10 s delay between repetitions. A total of 180 scans were recorded for each sample. The chemical shift values were referenced to 85% phosphoric acid (H_3PO_4).
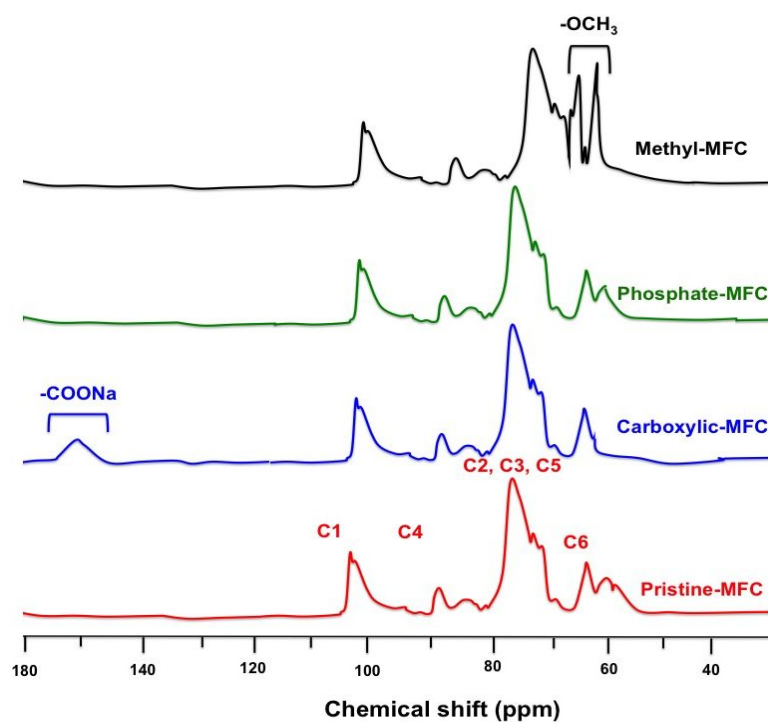

Figure S6: ^{13}C CP/MAS NMR spectra of unmodified (pristine-CMF) and functionalized-CMF. All carbons (C1, C2, C3, C4, C5, and C6) have been reported in this[13]C CP/MAS NMR spectra, and displacement after functionalization using various chemicals was also recorded.

The ^{13}C CP/MAS NMR studies were carried out to elucidate the possible reaction mechanism and region-selectivity (**Figure S5**). For the original CMF, the typical

signals of CMF appear at 107 ppm (C1), 76 and 73 (C2, C3 and C5) and 66.6 and 64.4 ppm (C6). A new peak at 176 ppm is ascribed to the sodium carboxylate carbons in the oxidized cellulose when compared to pristine-CMF. These results are consistent with the previous relevant report[14]. Carboxylic-CMF had nearly no influences on the chemical shift and the pattern of C1 or C4 in solid state ^{13}C CP/MAS NMR. However, the oxidized CMF has large resonance peaks due to the original C6 primary alcohol groups of the glucose at about 67.3 ppm. Meanwhile, the signal at 64.4 ppm for C6 carbon sharply decreases and disappears when it is compared with the pristine-CMF, which indicates selective oxidation of the primary OH-units.

Furthermore, the influence of NaClO volume on functionalization was determined. **Figure S6** indicates the possible fluctuation in the observed peaks. Slight decrease in 176 ppm was observed after an increase in NaClO volume.
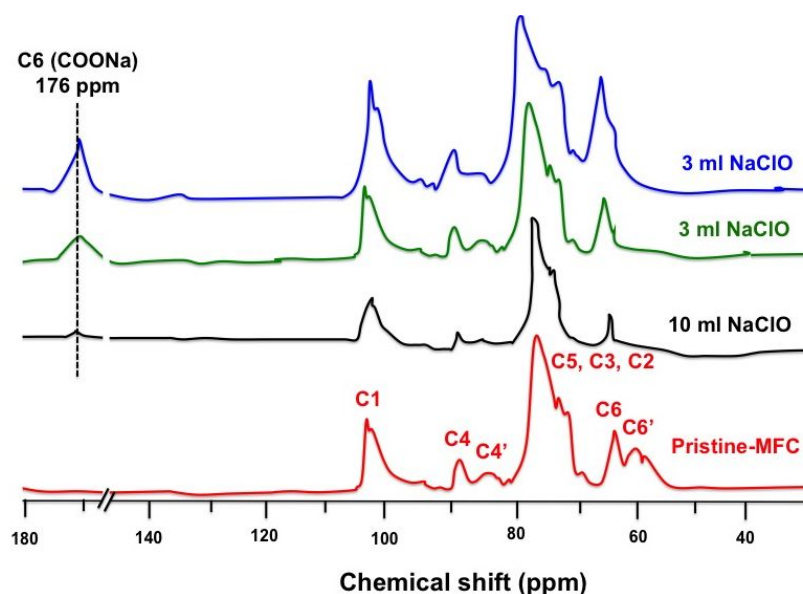
Figure S7: Effect of NaClO on carboxylation of CMF

As can be seen from the spectra (**Figure S5**), the noticeable signals within the region between 50 and 110 ppm can be defined as being mostly attributed to different carbons of cellulose: the region at58-68 ppm is assigned to C6 (i.e. C6 is a crystalline and C6' is an amorphous cellulose). The cluster of signals at 68-80 ppm can be assigned to C2, C3 and C5, respectively; the region at 80-91 ppm assigned to C4 (i.e. C4 is crystalline and C4' is amorphous cellulose), and finally the region at 101-109 ppm can be assigned to C1. After both, the heterogeneous and homogeneous, the phosphorylation reactions' changes within the spectrums could be observed of position C4 and C6. By comparing the spectra of hexokinase-ATP treatment with

increasing $MgCl_2$ concentrations results in more extensive structural changes and increase the spectral complexity of the pristine-CMF. The chemical shift observed for C6, which moved from 65.5 to 55.2 ppm after its substitution by the phosphate group. By spectral de-convolution and fitting the C6 signal with three to five Lorentzian lines, it is possible to separate the integrated signal intensity assigned to crystalline cellulose from the total signal intensity of the C6 range.
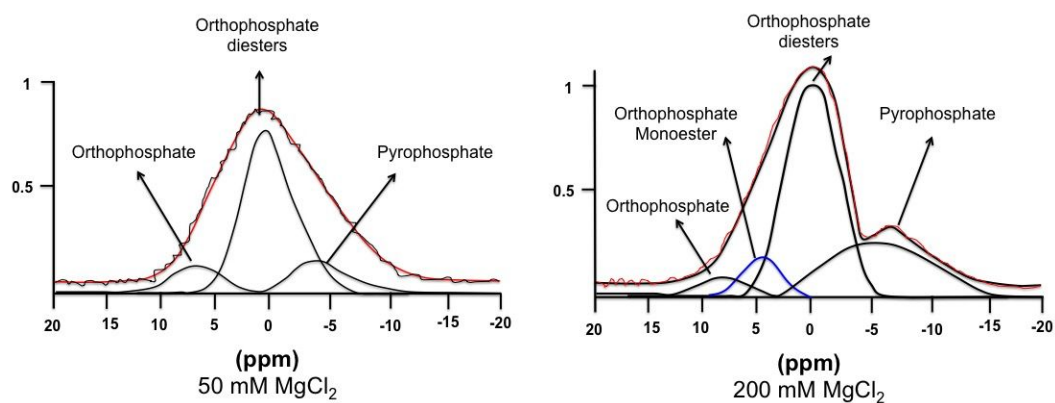
Figure S8: ^{31}P MAS NMR spectra of phosphorylated-CMF using 50 and 200 mM $MgCl_2$ at 50 mM ATP and 35 U/ml of hexokinase

Furthermore, when using 200 mM $MgCl_2$, the highest DS value was obtained, and the chemical shift of C6 bearing OH groups available for substitution was shifted, and the amorphous spectral part split, thus confirming that phosphorylation only occurred at the C6 position.

The pristine-CMF did not show any peak (data not shown), whereas the spectrum of phosphate-CMF using 50 and 200 mM $MgCl_2$ showed clear peaks within the range of +15 to -15 ppm (**Figure S8**). This shift is typical for phosphoric mono- and diesters, and thus confirmed the presence of the phosphoric ester in CMF. The peaks of the solid-state spectrum are broad, each of which overlaps the chemical shifts of several P nuclei. However, peak identification and quantifications in the spectra can again be improved with their de-convolution resulting to three peaks, at samples being treated with 50 mM $MgCl_2$, corresponding to the orthophosphate, orthophosphate diesters and pyrophosphate, respectively. Whereas in the case of using 200 mM $MgCl_2$ four peaks were identified, i.e. peaks at 7.0, 4.4. 1.8 and -6.3 ppm corresponding to the orthophosphate, orthophosphate monoester, orthophosphate diesters, and pyrophosphate, respectively[15].

The methylated samples have four resonance lines divided into three different spectral ranges (105, 85/75 and 60 ppm), which can be distinguished in the ^{13}C NMR spectrum. The C1 carbon signals for methyl-CMF samples appear in the same resonance line of cellulose at 105 ppm. Carbons C2, C3, C4 and C5 signals appear in the double peak region at 85 and 75 ppm. However, if C6 is substituted, these C6 resonances also fall into this spectral range. Finally, the signals of all unsubstituted C6 carbons and of all methyl groups, replaced in the methylation, compose the resonance line around at 60 ppm (**Figure S6**).

4.6. XRD analysis:

X-ray diffraction measurement was performed on a D/max III X-ray diffractometer (Rigaku Tokyo, Japan), equipped with nickel-filtered Cu Kα radiation (λ = 0.15418). The diffraction angles (2θ) ranged from 5° to 40°, and the step size was 0.04^{o}. A Lorentzian deconvolution was used for peak separations. The d-spacing (d) of the produced nanolaminate membranes were calculated with the Bragg equation[16]

$$d = \lambda/2\sin\theta \ldots\ldots\ldots\ldots\ldots\ldots\ldots\ldots\ldots\ldots\ldots\ldots\ldots\ldots Eq (1)$$

Where λ is the wavelength of X-ray source (0.15418) and θ is the Bragg angle corresponding to the plane.

Table S3: lamellar structure of functionalized CMF membranes

| MFC Sample	Interlayer Spacing d (Å)	Bond Length (Å)
Pristine	3.9	O-H = 0.97
Carboxylate	+1.7	C=O-O = 1.20-1.34
Phosphorylated	+4.7	P=O = 1.56
Methylated	+4.1	C-H = 1.09

4.7. XPS analysis of functionalized CMF:

The X-Ray photoelectron spectroscopy analyses were carried out on the PHI-TFAXPS spectrometer produced by Physical Electronics Inc. The analyzed area was 0.4 mm in diameter, and the analyzed depth was about 3-6 nm. The sample surfaces were excited by X-ray radiation from a monochromatic Al source at a photon energy of 1,486.6 eV. The high-energy resolution spectra were acquired using an energy analyzer operating at a resolution of about 0.65 eV and pass-energy of 187 eV. During data processing the spectra from the surface were aligned by setting the C–C/C–H peak in the C 1 s spectrum to a binding energy of 285.0 eV. The accuracy of the binding energy was about ± 0.3 eV. The concentrations were calculated from the intensities of the peaks within the XPS spectra using relative sensitivity factors provided by the instrument's manufacturer. Two spots were analyzed on each sample, and the average composition was calculated.
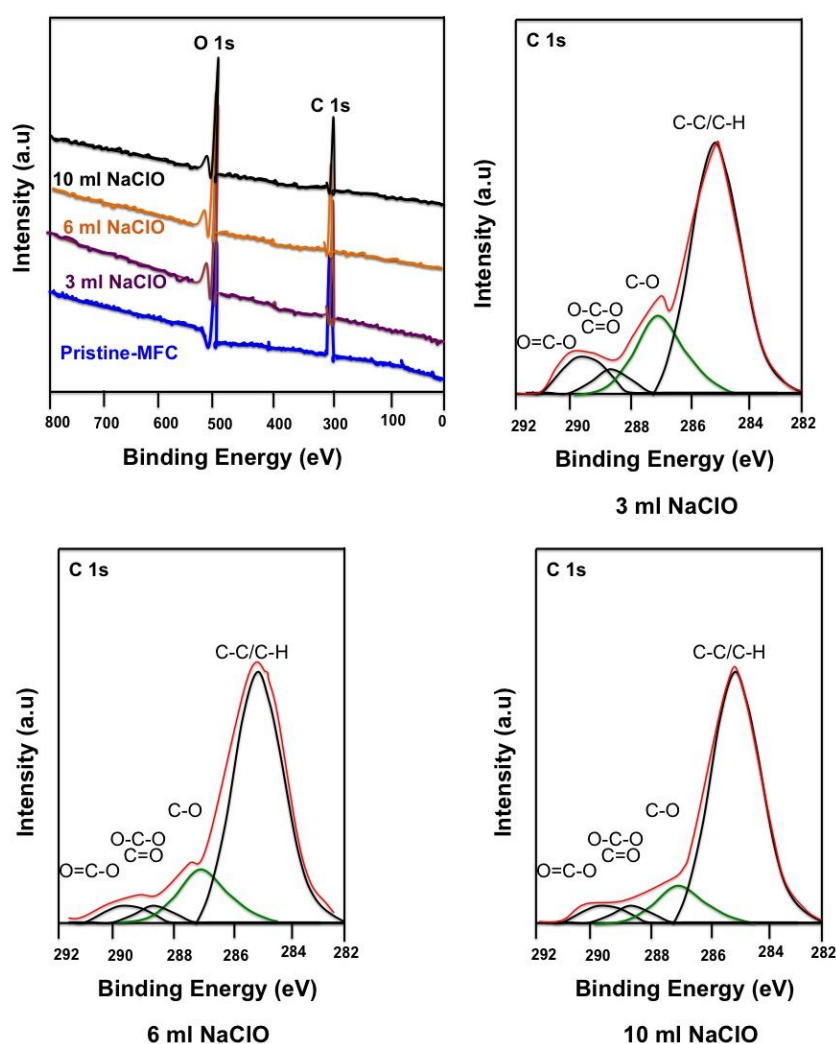
Figure S9: (A), Survey XPS core level spectrum of pristine and carboxylated-CMF using different concentration of NaClO
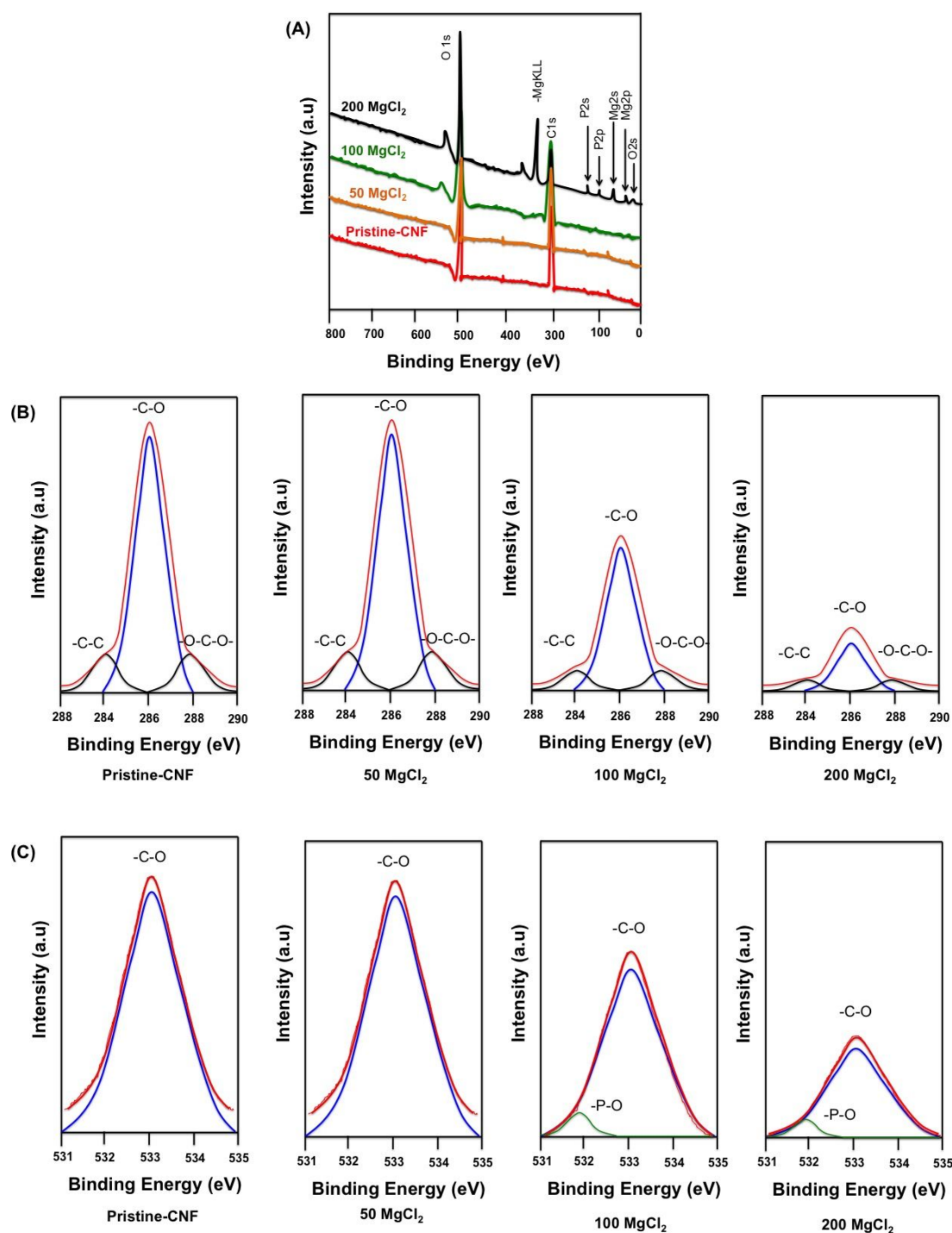
Figure S10: (A), Survey XPS core level spectrum of pristine and phosphorylated-CMF using different concentrations of MgCl$_2$. **(B)**, High-resolution scans of C1s of native and modified-MFC. **(C)**, High-resolution scans of O1s of native and modified-CMF.
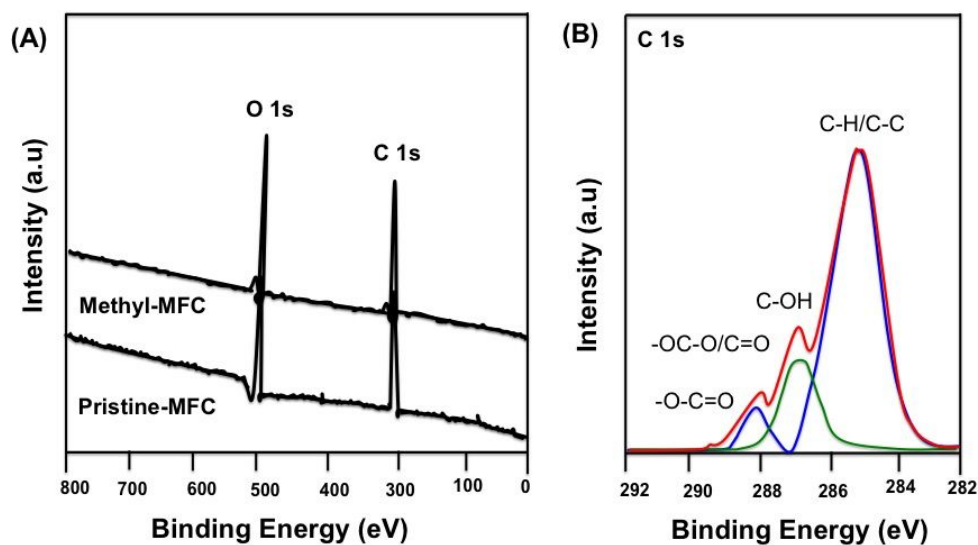
Figure S11: Methylation of CMF. **(A)**, Survey XPS core level spectrum of pristine and methylated-CMF and **(B)**, high-resolution scans of C1s of native and modified-CMF (methylated)
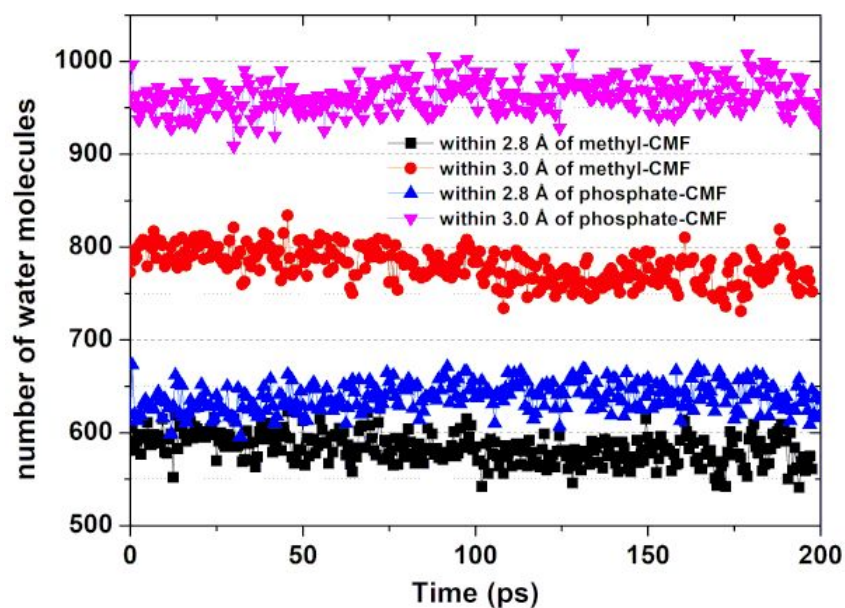
Figure S12: Computational simulations of the solvation effect on methylated and phosphorylated CMF (when they are not dried but evolving in solution). Here we can see the trend of the water content (number of water molecules within 2.8 and 3.0 Å of the fibers) during the last portion of the dynamics (and the distribution)

When the chains of phosphate-CMF are extended their length is comparable to that of the methyl groups (practically, we have a broad distribution of chain lengths) but the degree of bending depends on the interactions of the various headgroups with the groups close by (these could belong to other fibers as well).

The interlayer spacing is determined by the type and strength of these interactions. In the case of methyl groups, they seem more repulsive than in the other case (especially when the methyl moieties are face-to-face). We should also consider the fact that methyl groups are more hydrophobic than phosphate groups (that are neutralized by counterions and solvated by water). The adsorbed waters (just a few molecules) play a sort of gluing effect between the fibers. These waters are almost absent in the case of methylated cellulose. Therefore, a greater separation between the fibers when we insert methyl groups seems more probable.

Furthermore, the *size* of the phosphate groups is larger than the one of the methyl groups. This could explain the tendency towards broader interlayer separations in the phosphate-CMF membranes. In **Figure 7** orange regions in methyl-CMF membranes indicate more open structures (i.e. a wider intercapilar spacing) compared to phophate-CMF membranes.

4.8. Water permeability:

Water permeability of all produced frameworks was calculated using Convergence Clean Water Flux (CWF) pilot system as shown in **Figure S11**. All produced frameworks were fixed in the module (size: 7 x 11 cm). First, membranes were fixed in the module, and all air bubbles were taking out by supplying water at low pressure (0.5 bar). The permeate flow rate was monitored using a high precision balance. Water permeance of frameworks was recorded at defined pressure after reaching the equilibrium and reported as $Lh^{-1} m^{-2}$.
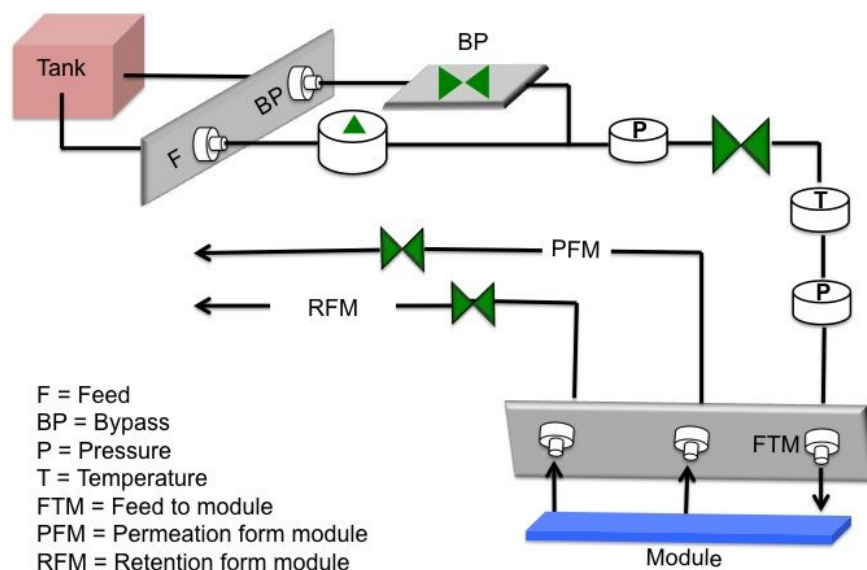
Figure S13: Convergence Clean Water Flux (CWF) pilot system was used for the measurement of water flux through the produced dimensional frameworks. Water flux was measured in continuous mode at a defined pressure. Membrane area used for measurement was ≈77 cm^2.

The highest water flux was recorded for the phosphate-CMF membrane, where the interlayer spacing was broader compared to other fabricated nanolaminate membranes. Considering that the grammage of the produced membranes is also essential for an efficient filtering process, it was interesting to disclose the effect of grammage on the water flux. An increase in the grammage of membranes determined a decrease in the water flux in all cases. The highest water flux was recorded for the phosphorylated-CMF membranes with a 50 g/m^2 grammage (**Figure 2C**).
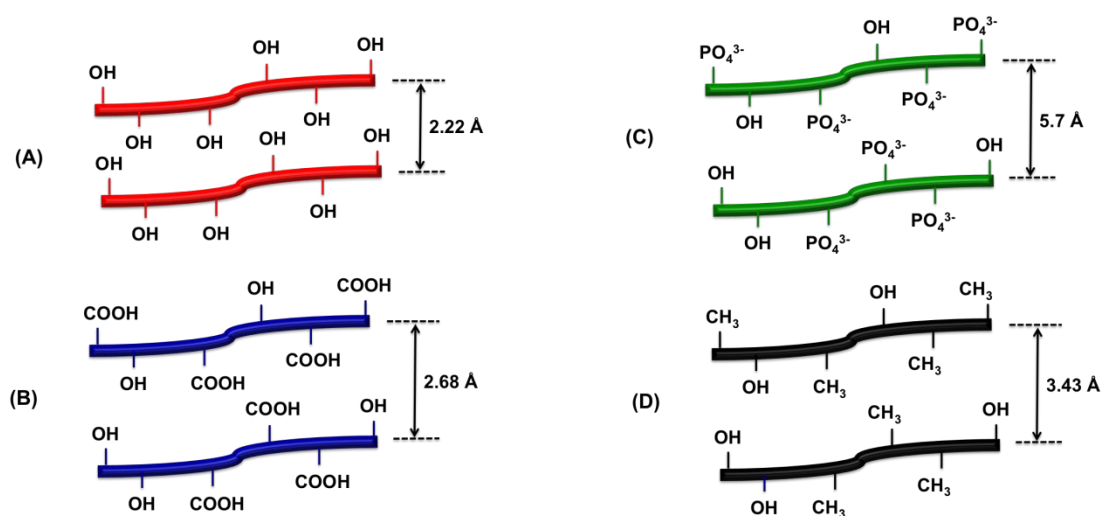
Figure S14: The increase in the inter-fiber spacing after the functionalization of CMF. **(A)**, Pristine-CMF has hydroxyl functional groups on the CMF surface. **(B)**, after TEMPO functionalization, carboxylic groups were introduced, thus, an increase in the inter-fiber spacing was observed according to the diameter of COOH groups. **(C)**, Highest inter-fiber spacing was obtained for phosphate functionalized CMF. **(D)**, Nonpolar attachment of methyl groups also increases the inter-fiber spacing between the fibers.

4.9. BET measurement: Pore-size distribution and average pore size of nanolaminate composite membranes were measured using a Micromeritics ASAP 2000 instrument, and the samples were degassed at 100°C for 24h in dry N_2 flow prior to measurements. First, all produced membranes were cut into small pieces and > 2 g of each sample was used for measurement. The detailed explanation is discussed by Karim et al. [8].

Table S4: BET analysis of fabricated nanolaminated composite membranes

Membranes	Functional groups	BJH adsorption pore width (Å)	BJH desorption pore width (Å)
Prinstine-CMF	-OH	72	75
Caroxylic-CMF	-COOH	169	190
methyle-CMF	$-CH_3$	310	329
Phosphate-CMF	PO_4^{3-}	256	267

4.10. Mechanical properties and Air permeance: The tensile strength of all produced frameworks was measured using a tensile tester (Lorentzen &Wettre, ABB, Sweden), as discussed in our recently published article**.**

Air permeance of samples was measured using L&W air permeance tester (Lorentzen &Wettre, ABB, Sweden). First, calibration of the tester was performed, and then samples were placed under holder and defined air pressure was applied.

Table S5: All produced frameworks were tested in tensile mode and air permeance was calculated as shown above

Types of structures	Max stress (MPa)	Strain at break (%)	Modulus of Elasticity (MPa)	Air permeance (μm/Pa,s)
Pristine-MFC	38±2.7	3±0.4	22±1.2	2.4±1.1
Carboxylic-MFC	35±2.1	2±0.3	24±3.1	3.1±2.1
Phosphate-MFC	32±1.3	2±0.2	26±2.2	4.5±1.5
Methyl-MFC	34±4.5	3±0.3	21±3.7	4.1±2.9

5. Nanolaminated membranes performance:

5.1. Ions permeation rate:

We performed the measurements for different ionic strengths corresponding to the salt concentration of 0.5 M, 01.0 M, and 1.5 M in the feed side system (Dead-End-Cell system with low applied pressure). The 1 M of NaCl was selected for NaCl rejection experiment. The applied vacuum was 0.5 bar. The percentage removal was calculated using equation given below

Percentage removal = C_f - C_p/C_f x 100……………………………….(i)

Where C_f is the concentration of feed, C_p is the concentration of permeate used in the measurements.

5.2. Membrane performance for removal of metal ions, dye, and drugs

The polluted water contaminated with metal ions was collected from an industrial site in Örnsköldsvik, Sweden. The concentration of metal ions in the contaminated water is given in **Table S6**. Table S6 further demonstrates the percentage removal and capacity of used nanolaminate membranes.

Table S6: Treatment of wastewater using functionalized nanolaminate composite membranes

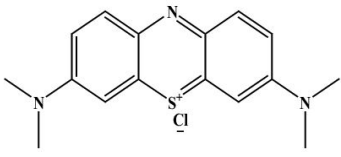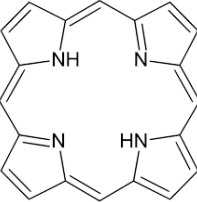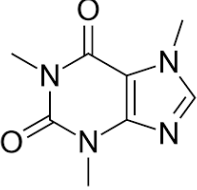| Functionalized membranes	Removal (%)				Removal capacity (mg/g)			
	C_o (µg/L)							
	Mg^{2+} (5800)	Cd^{2+} (5.77)	Co^{2+} (1.03)	Cr^{3+} (9.87)	Mg^{2+} (5800)	Cd^{2+} (5.77)	Co^{2+} (1.03)	Cr^{3+} (9.87)
Pristine-MFC	7	39	26	30	165	250	198	221
Carboxylic-MFC	55	60	39	38	254	369	250	290
Methyl-MFC	48	27	34	20	244	200	188	190
Phos-MFC	67	81	75	80	364	544	370	454

All metal ions were removed in cross-direction flow using Dead-End-Cell apparatus as discussed in our previous published article[4]. The known amount of polluted water is filled in Dead-End-Cell column (300 ml) and passed through the used functionalized nanolaminate membranes. Percentage removal was calculated using equation (i). Capacity of used functionalized membranes was also calculated as mentioned below.

Co-Ci x V/W………………………………………………..(ii)

Where Co and Ci are initial and remaining concentrations of metal ions in mg/L^{-1} and V is the volume in liters and W is weight in grams of composite mmebranes.

**Table S7:** Contaminants details used for removal studies

Contaminants	Metal ions (µg/L)			Ref.
	Structure	Molecular weight (g/mole^{-1})	Stock radius (Å)	
Mg^{2+} (5800)	Nil	24.305	0.86	Karim et al.[17]

Cd^{2+} (5.77)	Nil	112.4	0.95	
Co^{2+} (1.03)	Nil	58.9	0.88	
Cr^{3+} (9.87)	Nil	**51.9**	0.75	
Molecular dye				
Methyl blue		799,8	12.5	Karim et al.[8]
Drugs				
Porphyrin		310.3	270	Ribeiro et al.[18]
Caffeine		194.2	3.87	Price et al.[19]

Dye concentration of 15 mg/L was prepared in pH 5.0 in stock. The selected concentration was the highest limit in an industrial effluent, as discussed with the paper and pulp industry. Treatment experiments were performed in static as well as in dynamic mode. In static mode, nanolaminate composite membranes were incubated with model polluted water for 24 h (saturation limit), and then percentage adsorption was calculated by applying equation (i). Rejection percentage of dye was calculated in dynamic mode. The experiment was performed as discussed for the metal ions removal section. The high percentage rejection of composite membranes in dynamic mode might be due to a large number of functional groups available for the immobilization of molecules dye.

The effect of pH on the removal of molecular dye was observed, and the obtained results are reported in **Figure S15**. It has been found that obtained zeta-potential of produced nanolaminate membranes have a direct influence on the adsorption of molecular dye. An increase in adsorption percentage was recorded with a decrease in zeta-potential of fabricated membranes (**Figure S3**).

Concentrations of drugs used for the rejection study were 1 M. Both drugs were dissolved in a buffer solution having pH 5.0, and all rejection experiments were performed in dynamic modes as discussed in the case of metal ions and molecular dye rejection studies. The percentage of rejection was calculated by applying equation number (ii).
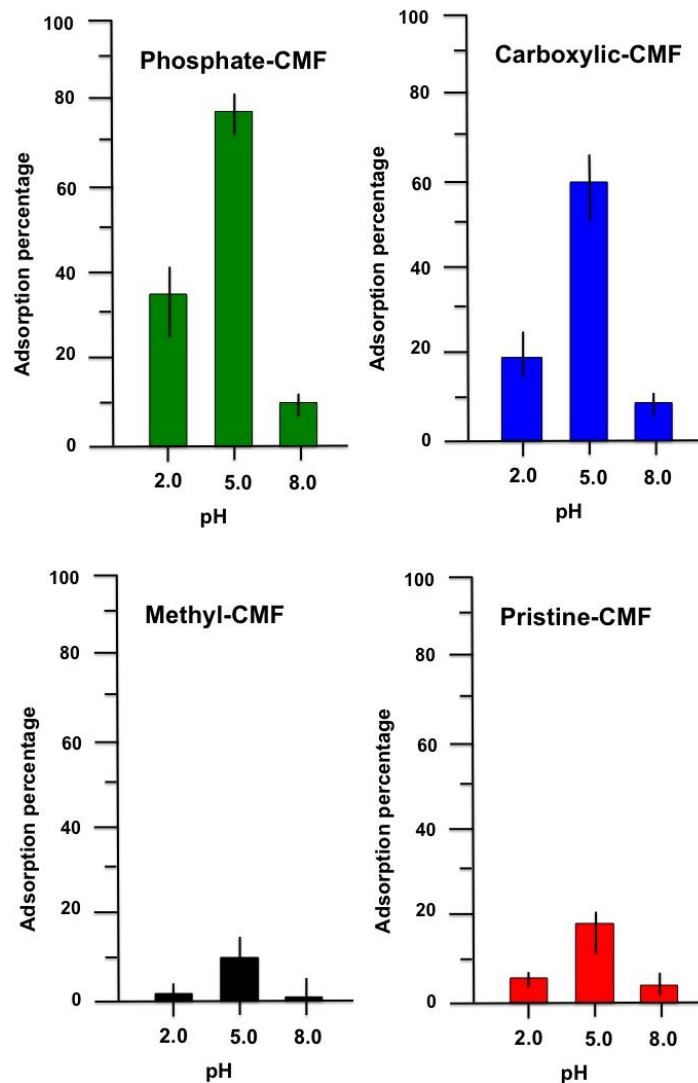
Figure S15: The effect of pH on the adsorption of dye was analyzed. Higest removal was observed for phosphate-CMF followed by carboxylic-CMF, pristine-CMF, and methyl-CMF.

6. Model Building and Simulation Details:

The nanocellulose (CMF) model is made of sixteen chains, which contain sixteen glucosyl residues each. They were shaped as a parallelepiped rod (approximately 84 x 26 x 26 Å^3) and modified according to the experimental conditions, by replacing the —CH$_2$OH groups exposed to the solvent with carboxyl (carboxylate-CMF), phosphate (phosphorylate-CMF) and methyl (methylate-CMF) moieties. The percentage of functionalized groups was based on experimental data. The resulting negatively charged systems were then neutralized by adding positively charged counterions (Na$^+$ and Ca^{2+}) and solvated by surrounding them with approximately 15000 water molecules (simulation box size: 84 x 101 x 54 Å^3). The initial configurations were equilibrated, preliminarily, in the NPT ensemble at T=300K for about 200 ps. Periodic boundary conditions were applied in all directions in such a way that the replication along x emulated a continuous infinite nanofiber.

The size of the system was appropriate to generate a reasonable variety of geometries with the different functionalizations useful for explaining and predicting the results of the experiments.

A preliminary simulation, approximately 500 ps long, was employed to generate a few different starting structures, which were then used to extend the sampling in each case. The total simulation time, which was around 5 ns, was sufficient to obtain relatively stable arrangements. The final analysis was focused on the last portions of the trajectories.

During the equilibration stage, carried out in the NPT ensemble at T=300K, constraints were applied to the solute and to the x dimension of the box to guarantee continuity, then the constraints were removed, and the simulations were extended saving the structure every 0.4 ps. The temperature was controlled through Berendsen's thermostat[20] with a relaxation constant of 0.1 ps, and the time step was set to 0.5 fs. All reactive molecular dynamics runs were based on a previous parametrized force field tuned for these systems[21] and carried out with the ReaxFF

code available in the Amsterdam Density Functional (ADF)/ReaxFF package [E. J. Baerends et al. ADF, adf2014.05[22] installed on local clusters and workstations (at CNR-ICCOM/IPCF). The primary sampling was obtained through the LAMMPs package available at the CINECA supercomputing center (high-performance computing resources - ISCRA initiative).

The analysis of the last portion of the production trajectories was focused on the comparison of the three different models. The reorganization of the CMF chains was accomplished by checking the root mean squared deviations of the atoms relative to the average structure (calculated from the last hundred-picoseconds of the productions). The relative positions of the metal ions were examined in detail together with hydrogen bonds, protonation states, and solvation effects. Visual inspection of the trajectories was also useful to disclose the orientations of the functionalizing moieties and their elongation into the solvent.

To evaluate the packing capability of CMF, due to the different functionalizations, the final average configurations were dried by a two-step procedure. First, all the water molecules far from the CMF interface were removed, and the system was compressed, then it was equilibrated in the NPT ensemble at T=300K. Second, only those water molecules within 2.5 Å of the CMF chains were retained, and the system was equilibrated again through a protocol similar to the first one.

It is worth mentioning that, due to the amorphous nature of the nanocellulose material in these complex environments and to the significant number of degrees of freedom, it is impossible, also by extending the number of models and the simulation times, to obtain fully detailed molecular models or more realistic representations of these supramolecular arrangements. Experimental characterization at the atomic level is likewise impossible, and only theoretical models can provide such descriptions deducing possible explanations of many of the effects observed experimentally. Although the complex aggregation and full stabilization of the CMF chains, water, ion, and counterions are very slow processes that cannot be fully disclosed with modeling (due to the extremely long simulation times - with the ion motion as the rate-determining step in the total convergence), the present simulations can provide explanations and ideas of the tendencies and trends of both the nanocellulose chains and the surrounding environment.
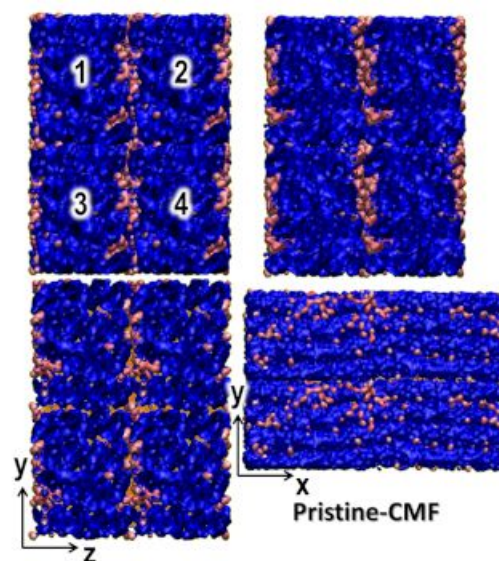
Figure S16. Packing of the dried fibrils models. The CMF fibers are rendered through the solvent-accessible surface, whereas water, channels, and cavities are displayed as orange areas. The numbers 1, 2, 3, 4 represent the replicated models, whereas the axes indicate the directions of the replication.

7. References:

1. A. Serra, I. Gonzalez, H. Oliver-Ortega, O., Tarres, M. Delgado-Aguilar, P. Mutje, Reducing the amount of catalyst in TEMPO-oxidized cellulose nanofibers: Effect on properties and cost. *Polymer*, 2017, **9**, 557-571.

2. M. Bozic, P. Liu, A. P. Mathew, V. Kokol, Enzymatic phosphorylation of cellulose nanofibers to new highly-ions adsorbing, flame-retardant and hydroxyapatite-growth induced natural nanoparticles. *Cellulose*, 2014, **21**, 2713-2726.

3. K. Junka, I. Filpponen, T. Lindstrom, J., Laine, Titrimetric methods for the determination of surface and total charge of functionalized nanofibrillated/microfibrillated cellulose (NFC/MFC). *Cellulose*, 2013, **13**, 2887-2895.

4. Z. Karim, A. Svedberg, K. Y. Lee, M. J. Khan, Processing-structure-property correlation understanding of microfibrillated cellulose based dimensional structures for ferric ions removal. *Sci. Rep.*, 2019, **9**, 10277.

5. T. L. Ogeda, I. B. Silva, L. C. Fidale, A. O. EI-Seoud, D. F. S. Petri, Effect of cellulose physical characteristics, especially the water sorption value, on the

efficiency of its hydrolysis catalyzed by free or immobilized cellulose. *J. Biotechnol.,* 2012, **157**, 246-252.

6. C. L. Chen, Methods in lignin chemistry. Berlin: Springer-Verlag, PP. 465-471 (1992).

7. R. G. P. Viera, G. Rodrigues Filho, R. M. N. de Assuncao, C. S. Meireles, J. G. Vieira, G. S. de Oliveira, Synthesis and characterization of methylcellulose from sygar cane bagasse cellulose. *Carbohydr. Polym.*, 2007, **67**, 182-187.

8. Z. Karim, A. P. Mathew, M. Grahn, J. Mouzon, K. Oksman, Nanoporous membranes with cellulose nanocrystals as functional entity in chitosan: removal of dyes from water. *Carbohy. Poly.*, 2014, **112**, 668-676.

9. Z. Karim, M. Hakalahti, T. Tammelin, A. P. Mathew, A. P., Oksman, K. *In situ* TEMPO surface functionalization of nanocellulose membranes for enhanced adsorption of metal ions from aqueous medium. *RSC Adv.*, 2017, **7**, 5232-5241.

10. A. Isogai, T. Hänninen, S. Fujisawa, T. Saito, Review: catalytic oxidation of cellulose with nitroxyl radicals under aqueous conditions. *Progress poly. Sci.*, 2018, **86**, 122-148.

11. D. M. Suflet, G. C. Chittanu, V. I. Popa, Phosphorylation of polysaccharides: new results on synthesis and characterization of phosphorylation cellulose. *Teact. Funct. Polym.*, 2006, **66**, 1240-1249.

12. R. L. Oliveira, J. G. Vieira H. S. Barud R. M. N. Assuncao, G. R. Filho, S. J. L. Ribeiro, Y. Messadeqq, Synthesis and characterization of methylcellulose produced from bacterial cellulose under heterogeneous condition. *J. Brazilian Chem. Sco.*, 2015, **26**, 167-174.

13. M. Ghanadpour, B., Wicklein, F. Carosio, L. Wågberg All-natural and highly flam-resistant freeze-cast foams based on phosphorylated cellulose nanofibrils. *Nanoscale*, 2018, **10**, 4085..

14. T. Saito, I. Shibata, A. Isogai, N. Suguri, N. Sumikwa, Distribution of carboxylic groups introduced into cotton linters by TEMPO-mediated oxidation. *Carbohyd. Poly.*, 2005, **61**, 414-419.

15. B. L. Cade-Menum, Characterization of phosphorous in environmental and agricultural samples by ^{31}P nuclear magnetic resonance spectroscopy- *Talanta*, 2005, **66**, 359-371.

16. C. Montero, B. Clair, T. Almeras, A. V. D. Lee, J. Gril, Relationships between wood elastic strain under bending and cellulose crystal strain. *Comp. Sci. Technol.*, 2012, **72**, 175-181.

17. Z. Karim, D. Georgouvelas, A. Svedberg. A. P. Mathew, Pilot scale engineering of microfibrillated cellulose (MFC) flat sheet membranes for removal of changed water pollutants. *Carbohy. Poly.*, (2020) (submitted)

18. A. C. F. Ribeiro, M. C. F. Barros, L. Verissimo, C. Santos, Diffusion coefficients of paracetamol in aqueous solutions. *J. Chem. Thermodyn.*, 2012, **54**, 97–99.

19. W. E. Price, Tracer caffeine diffusion in aqueous solutions at 298 K. The effect of caffeine self-association. *J. Chem. Soc. Faraday Trans. 1 Phys. Chem. Condens. Phases*, 1989, **85**, 415–419.

20. H. J. C. Berendsen J. P. M. Postma, W. F. van-Gunsteren, A. DiNola, J. R. Haak Molecular Dynamics with coupling to an external bath *J. Chem. Phys.*, 1984, **81**, 3684-3690.

21. C. Zhu, S. Monti, A. P. Mathew, Cellulose nanofiber–graphene oxide biohybrids: disclosing the self-assembly and copper-ion adsorption using advanced microscopy and ReaxFF simulations. *ACS Nano*, 2018, **127**, 7028-7038.

22. E. J. Baerends ADF, adf2016.106 SCM, Theoretical Chemistry, Vrije Universiteit, Amsterdam, The Netherlands, http://www.scm.com